Possible Dark Matter in the Galactic Center

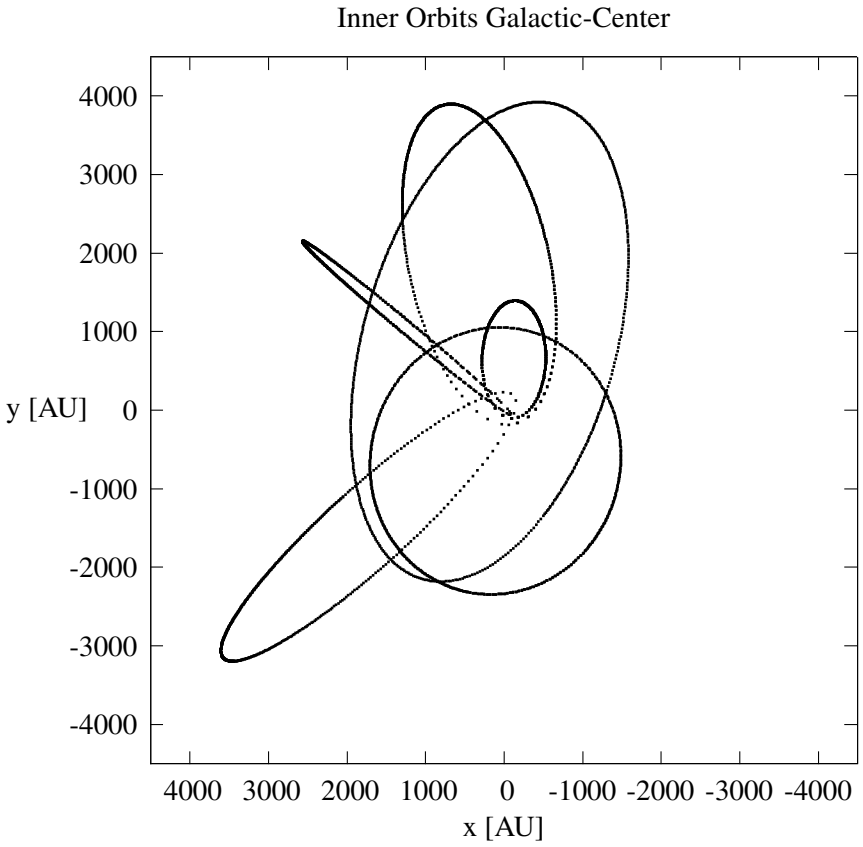

F.G. van Deuveren
August 2007

Supervisor: Dr. S. Portegies Zwart
@
Sterrenkundig Instituut Anton Pannekoek,
and
Section Computational Science

FACULTEIT DER NATUURWETENSCHAPPEN, WISKUNDE EN INFORMATICA

Abstract: The Galactic Center harbors a supermassive black hole (SMBH). The S-stars orbiting this 4.06×10^6 $M_\odot$ object are unaccounted for in standard models on starformation. The huge tidal field of the SMBH seems to contradict the presence of these young stars. This "Paradox of Youth" can be explained by the inspiraling cluster scenario. However, this implies that an IMBH is, or merged with the SMBH, or present in the vicinity of the SMBH. The latter is restricted by the mass and phase-space coordinates of the IMBH. There an IMBH is not observed at the Galactic Center, we found an upper limit of $\sim 10^4$ $M_\odot$ for the IMBH to avoid detection. This is of the same order as the lower limit on the mass necessary to transport the S-stars to their observed positions. Therefore we cannot exclude the inspiraling cluster scenario as an origin of the S-stars.

Contents

Chapter 1

Overview of the Galactic Center

1.1 Introduction

Figure 1.1: Galactic Center
Image of the Galactic Center from the Spitzer Telescope IRAC instrument. Infrared image with wavelength: 3.6 microns (blue), 4.5 microns (green), 5.8 microns (orange), 8.0 microns (red). Field of View: 1.9 x 1.4 degrees

The Galactic Center (GC) is by far the closest galactic nucleus, making it observationally one of the most promising parts of the Universe to study the phenomena related to this field of interest. The last decade, reasons have been found to assume the GC contains a Super Massive Black Hole (SMBH). Although, the dark mass

associated with this SMBH, could also be configured in other ways.

In this paper we will try to give more insight on the complexity of this intriguing part of our Galaxy. We will start this by giving an overview of the GC, in which we will emphasize the limitations and interpretations, of the available information. After this we will present an orbital model of 6 of the inner, so called, S-stars[1]. This will be done in a semi-analytical way and by a numerical method. Finally, the numerical model will be used to examine other configurations, of dark mass, possibly hiding in the GC.

1.2 Our Galaxy: The Milky Way

Let us start with the Milky Way. Its intrinsic size is about 100,000 light-years (ly), with the Sun located at ∼28,000 ly from the center[2] [Fig.1.2].

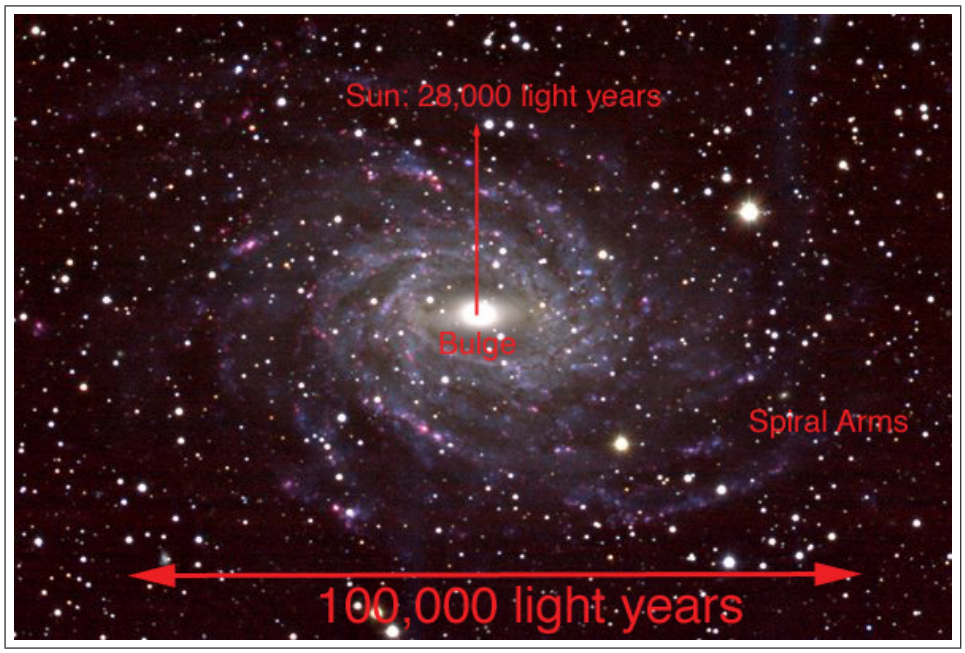

Figure 1.2: Size of the Milky Way

This is an image of NGC 6744. This galaxy is believed to be similar to our Milky Way. The diameter of the Milky Way is roughly 100,000 light years. The Sun is located about 28,000 light years from the center. In the center there is a bulge containing redder stars in comparison with the bluer stars located in the spiral arms.

[1] These 'inner' S-stars are within 1" offset from the Galactic Center

[2] More recent work shows the distance between the Sun and the GC more likely to be ∼26,000 ly (Reid [63])

With an age of 13.6 ± 0.8 Gyrs it is one of the oldest structures known and harbors both population I (young) and population II (old) stars (Pasquini et al. [55]). Estimations of its integrated absolute visual magnitude result in -20.9. With a mass of 5.8×10^{11} $M_{\odot}$ it comprises 200 to 600 billion stars (Battaglia et al. [6]). Nevertheless, most of the mass of the Milky Way is thought to be dark matter, spread out relatively homogeneously in a dark matter halo of an estimated 600 to 3000 billion solar masses (Battaglia et al. [6]).

The opaqueness of the central bulge shrouds our view of the GC in optical wavelengths. Peering through the interstellar dust, at other wavelengths, reveals more detailed characteristics of the Milky Way [Fig. 1.3]. Since we are going to focus our view on the GC, we will primarily use observational data obtained in the near infrared (NIR) and lower frequency part of the electromagnetic spectrum.

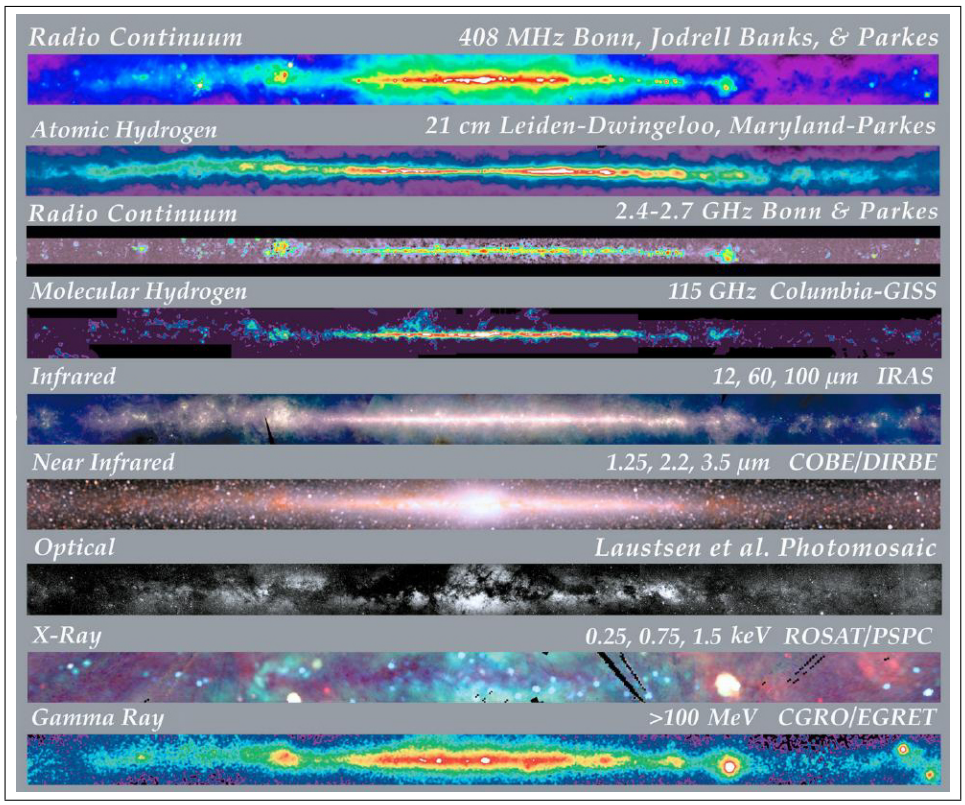

Figure 1.3: The Milky Way

Collection of images of the Milky Way in multiple wavelengths.

As a result of zooming into the GC, we will encounter several different units of size. This can easily raise confusion between the steps in size we take to reach the GC. Depending on the scope, of the field of interest, appropriate units of distance are used. Therefore, we present a conversion table with units which are commonly used in publications and throughout this paper.

	parsec	light-year	arcsecond[a]	AU
[parsec]	1	3.066×10^{-1}	3.879×10^{-2}	4.848×10^{-6}
[light-year]	3.262	1	1.265×10^{-1}	1.581×10^{-5}
[arcsecond][a]	25.783	7.905	1	1.250×10^{-4}
[AU]	2.063×10^{5}	6.324×10^{4}	8.000×10^{4}	1
[m]	3.086×10^{16}	9.461×10^{15}	1.197×10^{15}	149.598×10^{9}

Table 1.1: Conversion table for most commonly used distance units

The values placed vertically, between brackets, are the units after conversion. Conversion of units is based on the values: Julian year = 365.25 days = 31557600 s and c = 2.99792458×10^{8} ms^{-1}
Note[a]: The conversion of arcseconds is based on the distance to the Galactic Center $R_0 = 8.0$ kpc.

1.3 The Bigger Picture of the Galactic Center

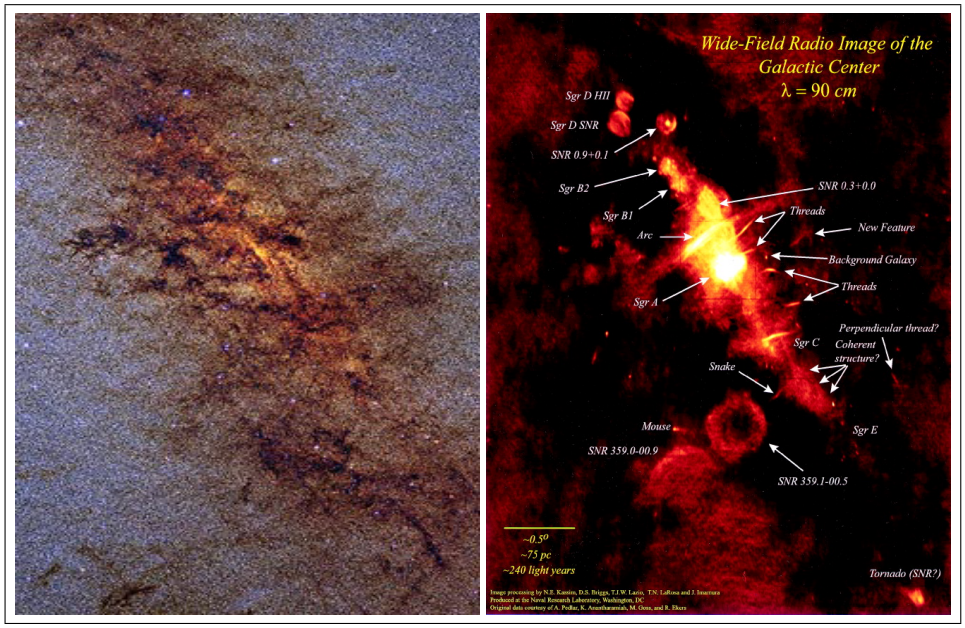

Figure 1.4: The Central Degrees

Near Infrared (2MASS) and Radio image (VLA) of the inner 2.50×4.00 degrees of the Galactic Center. On the contrary with the left, the right image reveals a numerous amount of features of the GC, notably Sgr. A^* in the center.

The GC is located in the constellation of Sagittarius. The bright radio source Sgr. A* is associated with an alleged SMBH at the center. As mentioned in the previous section, observations at optical wavelengths do not show very much variations at the GC. For several interesting phenomena even NIR observations are not sufficient to reveal their puzzling relationship with the GC. With the use of radio observations, we take a look at the outer structure of the Galactic Center.

One of the most striking aspects of the GC, at a scale of a few hundred parsec, is its magnetic field. Structures as non-thermal filaments , magnetic flux tubes and a large-scale, helically wound structure can be clearly distinguished from the background, see Fig. 1.4 (M. Morris [51]). At a closer level, see Fig. 1.6, one can see the intricate northern thread from Fig. 1.4, crossing with the thermal arches filaments, in Fig. 1.4 referred as Arc (Lang, Morris & Echevarria [41]).

1.3.1 The Outer Structure of the Galactic Center

With the improvement of resolution, of the observational instruments over the last decade, new features of the GC appeared. For example, within 100 ly from Sgr. A* we find two of the most dense stellar clusters known in the Milky Way (Figer et al.[22].

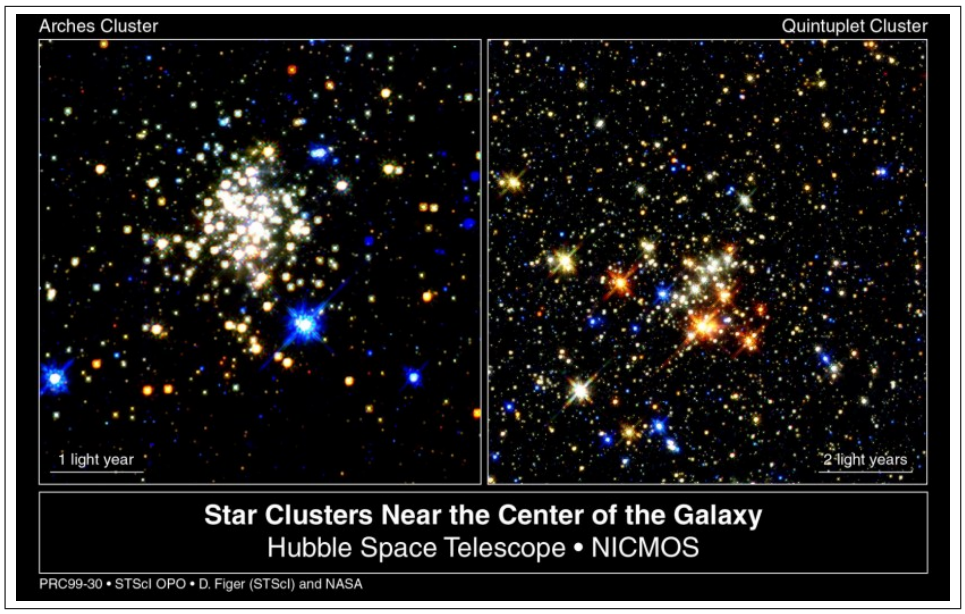

Figure 1.5: The Two most dense Clusters of the Milky Way

The Arches cluster (left) and Quintuplet cluster (right), two of the most dense stellar clusters in the Milky Way, are located in the Galactic bulge at less than 100 light years from the Galactic Center.

These clusters, the Arches and Quintuplet cluster, are at least 10 times more massive than typical young clusters. If we would compare the Arches cluster to the essentially empty space between the Sun and Alpha Centauri, our nearest neighbor, it would be filled with over a 100,000 stars [Fig. 1.5].

Zooming in even further, to a scale of a few parsecs, we find another feature of the GC. At a distance of $\sim$1 pc, a Circumnuclear disk (CND) orbits Sgr. A* with velocities of $\sim$110 km s^{-1}. This CND has an estimated typical mass of $2-3\times10^4$ $M_\odot$ and a total CND gas mass of $\sim 10^6$ $M_\odot$ (Christopher et al. [9]). It is assumed to act as a reservoir for future accretion activity onto Sgr. A*. Other disk like structures, which also have been observed, will be discussed int the next section.

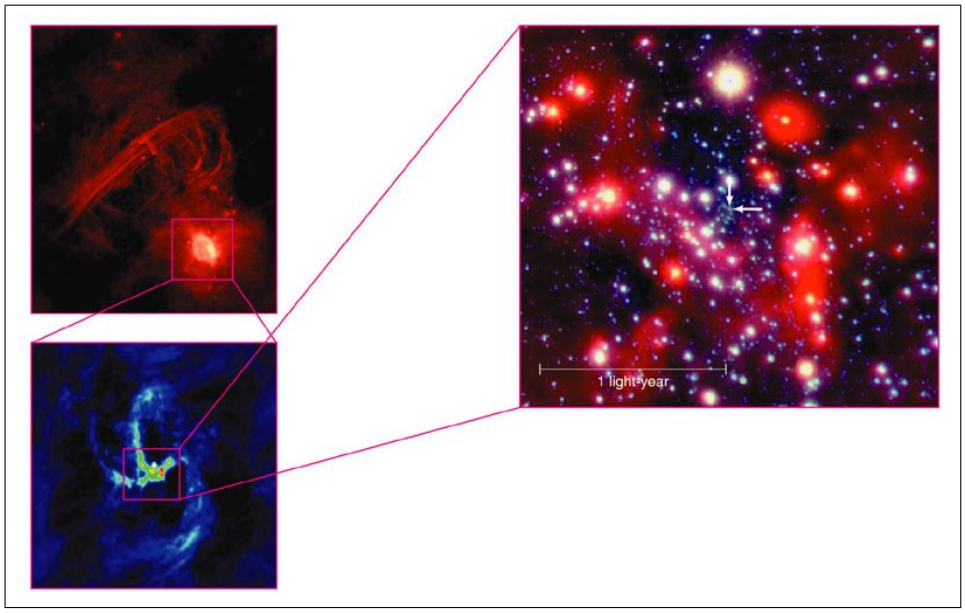

Figure 1.6: Towards the Central Parsec

Top Left: Centimeter wavelength image of the Galactic Center Radio Arc. The Radio Arc is connected to the Galactic center by strange curving filaments known as the Arches.
Bottom Left: Radio image (20 cm, VLA) image of the central $\sim$2.5 x $\sim$2.5 arcmin. containing Sgr A West, a spiral-like pattern of thermal ionized gas that appears to be falling into the very center of the galaxy. Right: A HKL color composite of the Galactic Center region. The location of Sgr. A* is marked by the two arrows.

1.3.2 Within 0.5 pc from Sgr. A*

Just over a decade ago, it became clear that the power output of the central half parsec ($\leq 10^5\ AU$) is dominated by young massive He-I stars (Krabbe et al. [39]). These young stars could not be explained by standard models of star formation due

to a huge tidal field, at $R = 0.1$ pc, of the central object. This tidal field was suggested to be induced by a dark mass of $\sim 3 \times 10^6$ $M_\odot$ which was very likely to be a very massive black hole. This alleged supermassive black hole (SMBH) is often referred as Sgr. A*. This raised the question, how can we explain the presence of these young stars in such an hostile environment? This became known as the "Paradox of Youth", we will discuss this separately in Section 1.5.

A few years later, in 1999, Eckart, Ott & Genzel ([19]) obtained accurate K-band spectroscopy of He-I, Brγ emission lines and CO absorption line. This resulted in these 'K'-stars, in the Sgr. A* stellar cluster, having almost no CO bandaged absorption. The Brγ emission line could be associated with the 'northern mini-spiral' [Fig. 1.6] rather than the Sgr. A* star cluster. This implicated that these K~ 14.5 stars should be classified as O9-B0.5 stars with masses of 15 to 20 $M_\odot$. In 2003, Genzel et al. ([25]), found that the stellar properties change significantly from the outer cluster (1"-10") to the dense innermost region around the black hole. The young massive outer cluster stars, were located in two disks which inclined at large angles and counter-rotating (Genzel et al. [26]). Because the stellar content of the disks showed strong similarities, we think that 5-8 million years ago, two clouds fell into the center and formed the two rotating disks.

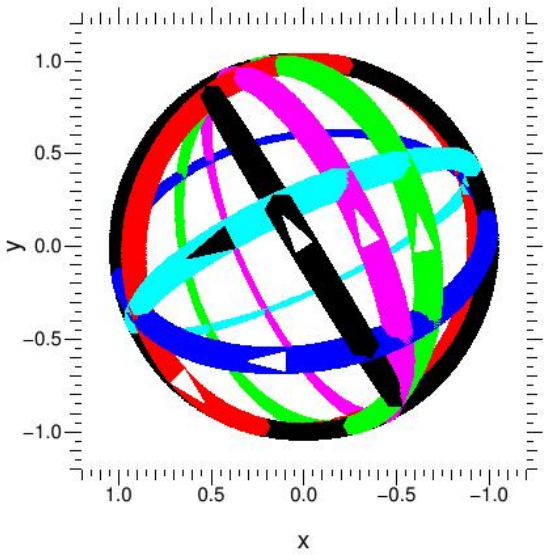

Figure 1.7: Planar Structures in the Galactic Center

Various planar structures in the GC: the Galaxy and sky (black), the clockwise (blue) and counter-clockwise (red) stellar systems, the Northern Arm (green) and Bar (cyan) components of the ionized mini-spiral, and the circumnuclear disk (CND) of molecular gas (magenta). Each plane is represented by one ring. Arrows indicate the direction of rotation (Paumard et al. [56]).

However, the numerical modeling of young massive stars in 0.1-0.2 pc, opened other possibilities. They where formed or at large distances from the Galactic center and underwent a fast inward migration. Or, these young massive stars where formed in situ in a massive self-gravitating disk. Though the latter, would require a possible but not common, top-heavy initial mass function (IMF) (Nayakshin et al. [53] and Nayakshin, Cuadra & Springel [52]).

More recent work, from Paumerd et al. [56], lead to the discovery of 40 new OB supergiants, giants and main sequence stars in the central parsec of the Galaxy. The identification of these stars contributed to the already known 80 OB stars in the central parsec(excluding the central arcsecond). Most of these stars reside in one of the two rotating disks. While, the stars of the 'OB star disk' show mainly circular orbits, the stars in the second disk exhibit primarily eccentric orbits. The several disk structures and their orientation are presented in Fig. 1.7.

The K-band luminosity function of the massive stars suggests a top-heavy mass function and limits the total stellar mass, contained in both disks, to be 1.5×10^4 $M_\odot$. The obtained data strongly favors in situ star formation from dense gas accretion disks for both stellar disks. Another recent study on these rotating disks in the gravitational field of Sgr. A*, shows the population does not longer exist at a distance ≤ 0.05 pc. Implying that these stars within cut-off radius, differ in origin and maybe stellar type, from those in the disks (Beloborodov et al. [5]). These 'inner' stars, which we will call S-stars, will be discussed separately in section 1.4.2.

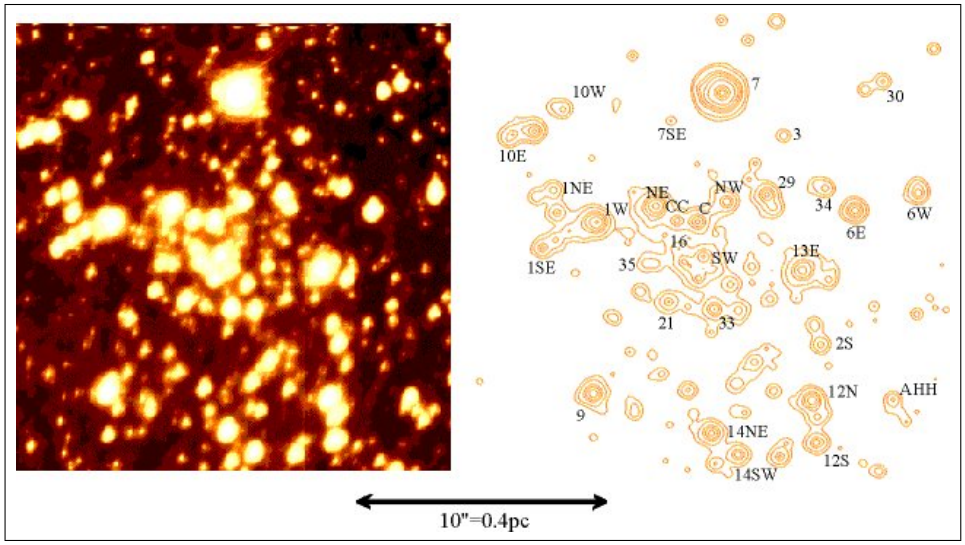

Figure 1.8: Collection of the Brightest Sources in the Central Parsec

Image of the brightest sources in the central parsec. On the right, the identifications of the stars in the left image. The brightest star is IRS 7 with a magnitude of 6.7. Sgr. A* is located just above the "SW" east of the IRS 16 cluster (East is to the left, and North is up).

A variety of very bright infrared sources (IRS) inhabit the central parsec [Fig. 1.8]. Among these is IRS 7 (6.7 mag), with a distance of 5.5 arcsec to Sgr. A*, the most luminous NIR source. Together with a large collection of SiO Masers, like IRS 9, Luminous Blue Variables (LBV) "candidates", IRS16NE and IRS16C, and a unclassifiable spectral type source IRS 3, this emphasizes the extraordinary environment around the GC (Martins et al. [46], Schödel et al. [67], Tanner et al [73]).

There is more known about these bright infrared sources, for instance co-moving groups of stars. Because of their similar proper motions the IRS 13E [Fig. 1.9] complex is an unusual concentration of massive, early-type stars (Schödel et al. [69]). After their discovery, this group was thought to be the remnants of a massive cluster containing an intermediate mass black hole (IMBH). Although, this is not likely on grounds of lacking evidence for a non-thermal radio and X-ray source in IRS 13E. Nevertheless, this intriguing object could tell us more about the origin of groups of stars in the vicinity of a SMBH. Numerical modeling of star formation in a gaseous disk, by Nayakshin et al. [52], showed an possible explanation for the origin of the stars around the GC. However, for the "mini star cluster" IRS13E, residing in the counterclockwise plane, there has not been found a possible scenario to explain it's presence.

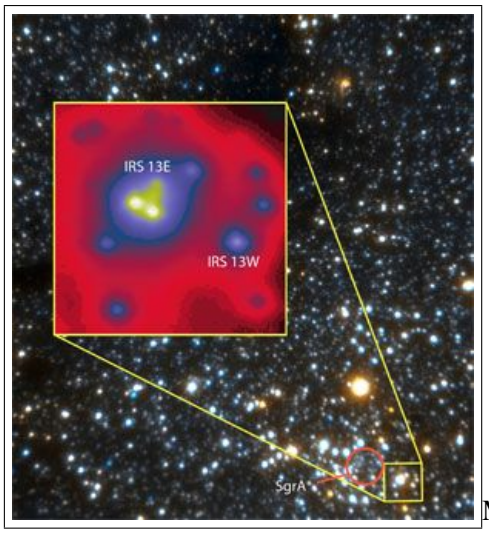

McMillan & O. Gerhard.

Figure 1.9: The IRS 13E Complex

A 40" x 40" Gemini Hokupa'a/QUIRC adaptive optics image of the region around the Galactic Center. Expanded view (5" x 3") shows IRS 13E and W from a deconvolved Kp band image (Maillard et al. [44]).

A second co-moving group of young stars was discovered by Lu et al. [43]. This group, called the IRS 16SW co-moving group, is located a factor of two closer to

the SMBH compared to IRS13. Most of the bright stars in the IRS 16 complex, including IRS 16SW are part of the clockwise disk, except for IRS 16NE and IRS 16NW which are part of the counter clock wise disk (Paumard et al. [56]). This co-moving group of stars is also believed to be a surviving core of a massive infalling star cluster. Recent work, from Martins et al. [46], showed IRS 16SW harbors a massive eclipsing binary. This binary system, GCIRS16SW, consists out of two $\sim$ 50 $M_{\odot}$ stars with an orbital period of 19.45 days. This makes this co-moving group of stars yet another intriguing mystery of the GC. An overview of the location of most of these phenomena can be found in Fig. 1.10.

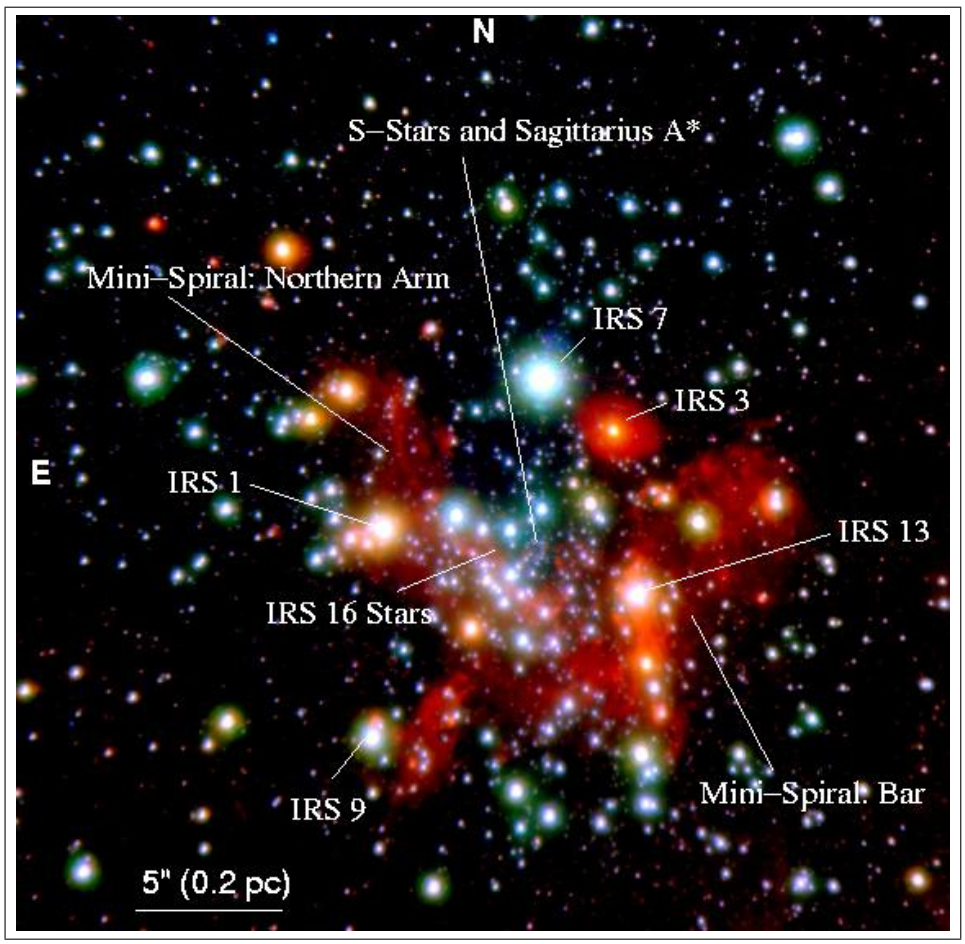

Figure 1.10: An overview of the Central Parsec

The central parsec of the Milky Way seen with the near infrared camera and adaptive optics system NACO at the ESO VLT. Two narrow band images (at 2.18m and 2.36m) were combined with a broad band image at 3.8m to obtain a pseudo-color image. The red extended emission is due to gas and dust in the mini-spiral or due to circumstellar material of individual stars.

1.4 The Inner Structure of the Galactic Center

The inner structure, within $\sim$1 arcsec, contains the two main ingredients for the research in this paper. The central mass (CM) and the stars, called S-stars, orbiting it. As stated earlier, the CM (SMBH) is often referred as Sgr. A*. In this section we will discuss these two features of the inner GC in more detail.

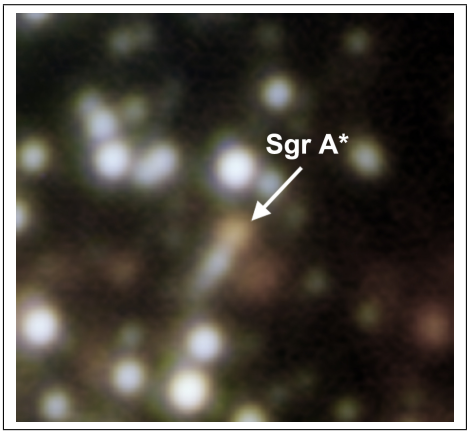

Figure 1.11: The Central Arcsecond

An HKL-band color mosaic of the central arcsec: H(1.8 microns) = blue, K'(2.2 microns) = green, L'(3.8 microns) = red. Observation has been done by the UCLA/Keck Galactic Center group.

1.4.1 The Central Mass and its Distance

The majority of observed quantities related to the CM, have an accuracy depending on the mass and distance to the GC, i.e. R_0. In 1993, Reid [63] set the distance to the Galactic Center to $R_0 = 8.0 \pm 0.5\,\text{kpc}$. Estimations, made in 1997, on the central dark mass resulted in 2-3 $\times\ 10^6\,M_\odot$ (Coker & Melia [11]). One year later diffraction-limited study, by Ghez et al. [29], resulted in a much better restrained estimation. Their work on the Galactic Center implicated a central mass of $2.6 \pm 0.2 \cdot 10^6\,M_\odot$. Because they also confined Sgr. A* within $\pm$0".1 ($\sim$ 800 AU), they suggested that due to the high mass to light ratio and high density there should be a central massive black hole. In addition to these results, they showed for the first time a large population of faint stars. The K-band images showed 90 stars with brightness ranging from $K = 9$ to $17\,mag$, and $2D$ velocities up to $1,400 \pm 100\,\text{kms}^{-1}$. These very fast moving stars are commonly known as hyper velocity stars (HVS).

Despite the anisotropic movement of the inner stars (within $\sim$ 1"), the isotropy of the stellar velocities induced the influence of a Spherical potential (Ghez et al.

[29]). An anisotropy-independent study of R_0 resulted in $R_0 = 7.8\text{-}8.2 \pm 0.9$ kpc, which is well inside the earlier stated boundaries (Genzel et al. [26]). Using Leonard-Merrit projected mass estimators and Jeans modeling they confirmed previous conclusions for a compact central mass $\leqq 10^{12.6}\,M_\odot$ dominates the potential between 0.01 and 0.1 pc.

In 2003, the first time also the independent movement of this central dark mass could be determined and putting it on $V_{CM} = 7.16$ to $8\,\mathrm{kms}^{-1}$ perpendicular to the galactic plane, giving $3 \times 10^6\,M_\odot$ within $100\,\mathrm{AU}$ (Reid et al. [62]). With the finding of Sgr. A* coinciding with the center of acceleration of S2, Schödel et al. [68], provided compelling evidence of Sgr. A* being a single SMBH. The evidence became even stronger when Ghez et al. [30], identified S0-16 within a mere 60 AU of the CM. The same year both the accuracy, in distance to the galactic center was improved to $R_0 = 7.94 \pm 0.42$ kpc (Eisenhauer et al. [21]), as in the mass estimations of the CM to $4.1\,(\pm 0.6) \times 10^6 R_0/8\,kpc^3\,M_\odot$ (Ghez et al. [31]).

By the use of better constrained orbits of the S-stars, the CM was pinpointed within 10 AU (Ghez et al. [27]). With this remarkable accuracy, the proper motion of the CM was set on $60 \pm 20\,\mathrm{kms}^{-1}$ in the galactic plane. In 2004, an infrared counterpart of the radio source Sgr. A* was found (Clénet et al. [10]). The alleged counterpart of Sgr. A* showed no significant short-term variability. The infrared spectrum of Sgr. A* was dominated by the synchrotron emission of non-thermal electrons, confirmed by the measurements of fluxes. Because, the emission arises away from the dynamical center of the S2 orbit, it would not originate from the closest regions of the black hole. When Ghez et al. [28], did the first Laser Guide Star Adaptive Optics (LGS-AO) observations of the Galactic center, Sgr. A*-IR showed strong intensity variations and during this observation no positional variations. They showed that the earlier positional variations could easily be explained by very red source, a locally heated dust feature.

In 2005, Shen et al. [71], showed Sgr. A* to be ~ 2 AU in size with VLBI observations at 7 mm, and with a radio image at 3.5 mm a size of ~ 1 AU. Resulting again in a new lower limit on the density of $6.5 \times 10^{21}\,M_\odot\,\mathrm{pc}^{-3}$, strengthening the case for a SMBH even more. Making it very unlikely there is not a SMBH at the center of our Galaxy. One of the most recent results is presented by Beloborodov et al. [5], who claimed that $M_{CM} = 4.3 \pm 0.5 \times 10^6\,M_\odot$ for $R_0 = 8.0\,\mathrm{kpc}$.

1.4.2 The Discovery of the S-stars

The other main 'ingredient' of the research of this paper are the S-stars in the vicinity of the SMBH. The S-stars at the Galactic Center have been mentioned several times. Due to the independent discovery of these stars, there can be some misunderstanding around their names and origin. Below we present a table with the variations, in using names, by different publicists.

Eisenhauer, Schödel, Genzel	S1	S2	S8	S12	S13	S14
Ghez, Weinberg	S0-1	S0-2	S0-4	S0-19	S0-20	S0-16
Paumard	E4	E1	E10	E5	E3	E2

Table 1.2: S-star name variations

Variations in name for S-stars as used by different publicists. The work in this paper will use the upper nomenclature of the S-stars

The isotropy of the stellar velocity field suggested the S-stars are moving under the influence of a spherical potential (Ghez et al. [29]). The fitting of a power law to the velocity dispersion $\sigma_{\rm v} \sim r^{\alpha}$ resulted in α -0.53 ± 0.1. This matches very well with Keplerian orbits which have $\alpha = -0.5$ (Ghez et al. [29]). The obtained K-band images showed 90 stars with brightness ranging from $K = 9$ to $17\,mag$, and $2D$ velocities up to $1,400 \pm 100\,\mathrm{kms}^{-1}$ (HVS). In 2000 it became clear that the inner, within 1 arcsec from the CM, S-stars differ from outer Sgr. A* star cluster. These inner S-stars showed radial or very elliptical orbits (Genzel et al. [26]).

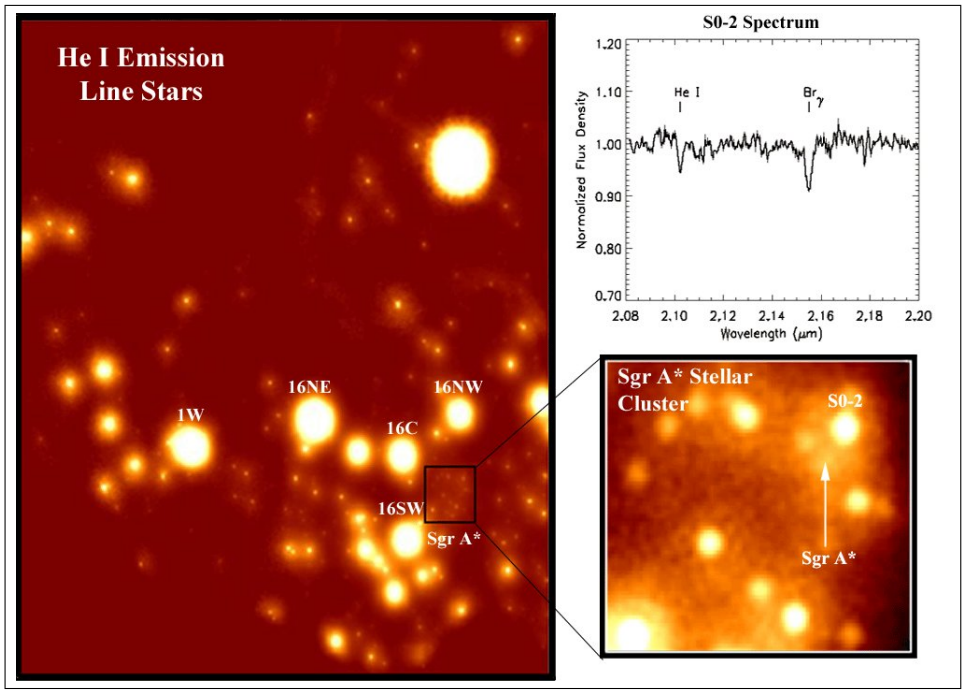

Figure 1.12: Milky Way

Left: A 7" x 10" K-band image scaled to show the location of the closest He-I emission line stars, which were the first stars to raise the debate of how star formation might proceed in the vicinity of the black hole. Bottom Right: A blow-up of 1" x 1" region containing the Sgr. A* cluster, a region centered on the black hole which shows a stellar density enhancement with stars that appear to be young and massive, that are an order of magnitude closer to the central black hole than the He-I stars, dramatically amplifying the problem of star formation in the vicinity of a black hole. Top Right: Spectrum of S2, which shows features that are consistent with an O9 main-sequence star.

In 2003 a precision of $\pm$ 0.2" or was reached, realizing an identification of S14 within 60 AU of the Central Mass (CM). Putting this "S"-star on an astonishing velocity of $9,000\,\mathrm{kms}^{-1}$ (Ghez et al. [30]). Observations on S2, 2.058 μm He-I, 2.165 μm Brγ resulted in S2 to being an O8-B0 dwarf with a mass of $15\,\mathrm{M}_{\odot}$, young ($\leqq$ 10 Myr) main sequence star [Fig. 1.12]. Later that year the uncertainties of the S-star Keplerian orbits were reduced with a factor 2 - 3 (Ghez et al. [31]). Again the question emerged about the "Paradox of Youth". Since S2 exhibited a 3.8 μm excess (L'-band) a stellar model of these "Super-blue stragglers" was presented (Genzel et al. [25]). Since the area where they are situated is a most hostile environment to give birth to new stars, it is most likely the formed through mergers and rejuvenated themselves.

In 2004, Ghez et al. [27], showed S14 orbited within 45 AU ($0.0002\,\mathrm{pc} = 600\,\mathrm{R}_s$). They published one of the first orbital fitted models, with the orbital parameters of the inner S-stars from a partially joint solution. But for this paper, the most important work was done by Eisenhauer et al. [20]. They presented an accurate fit to the orbital parameters of the inner 6 S-stars, showing the orbits in Fig. 1.13. The data presented by them is the basis of the research of this paper. The S-stars presented here are S1, S2, S8, S12, S13 and S14. These inner S-stars are being used to present a limit on possible dark mass configurations at the center of the Milky Way.

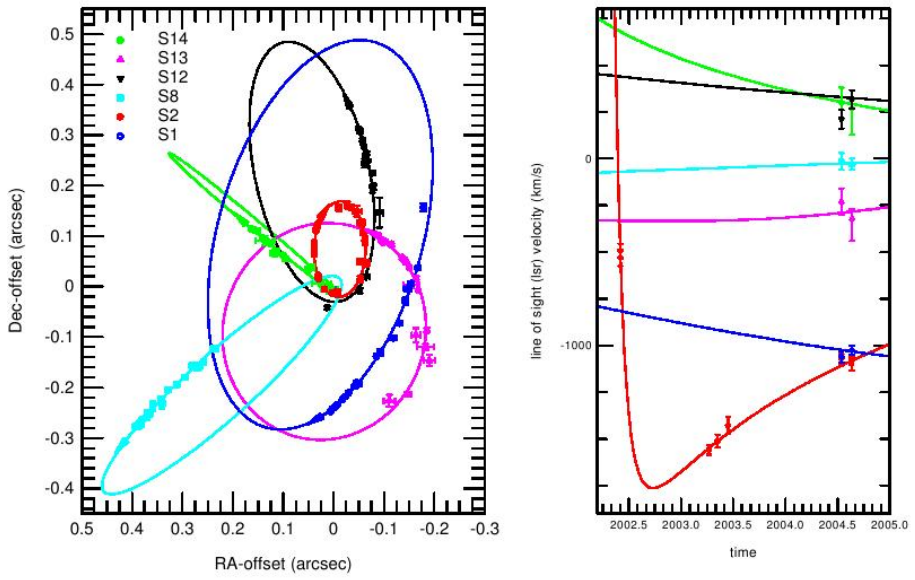

Figure 1.13: The Six Inner S-stars

Projection on the sky (left inset) and in time/radial velocity (right inset) of the 6 S-stars. The various color curves are the result of the best global fit to the spatial and radial velocity data of S1, S2, S8, S12, S13 and S14. The assumed distance is 8 kpc (Eisenhauer et al. [20]).

1.5 On the Origin of S-stars: "A Paradox of Youth"

As mentioned earlier, there are more then one unsolved problems at the GC. Maybe the most perplexing one, is on the origin of the S-stars. These S-stars, that have been observed within the central arcsecond, seem to be young massive stars. However, the SMBH at the GC induces such a strong tidal field that standard models of star formation rule out that these stars where 'born' in this neighborhood. This, together with the lack of old giants in the GC, is the so called "Paradox of Youth". Over the last years, several interesting solutions have been presented.:

1) Despite of the strong tidal field, the stars where formed in situ. Although this would require a top heavy IMF (Nayakshin et al. [53] & Nayakshin et al. [52]). This could be a solution for the outer stars, if gas would flow in periodically from the CND [42]. Using the idea of a self-gravitating disk together with Kozai's phenomena, Šubr & Karas [72] showed it was possible to get S-stars with high eccentricities. The S-stars then would have originated from self-gravitating disk with $M_{disk} \leqq 1\%$ of M_{SMBH}. However, gravitational instabilities in a massive disk show no starformation within 1" from the SMBH (Morris et al. [50]).

2) S-stars originating from massive stars by collisions and mergers (Genzel et al. [25]). A "collider model" in which the S-stars were formed and "rejuvenated" through mergers of lower mass stars in the dense central arcsecond. The collider model also accounts for the missing giants in the Sgr. A^* stellar cluster.

3) Another way to explain the presence of the S-stars is by assuming they are remnants of low to intermediate mass red giants. These red giants have been scattered into near-radial orbits around the GC. While approaching the black hole the gas, tidally stripped from the s-stars, could virialize with other s-stars orbiting the black hole (Davies & King [14]. The evolution, of the Sgr. A^* cluster or S-stars, by tidal stripping is limited by a dependence on a top heavy IMF, the scattering rate and a short relaxation time (Dray, King & Davies [15]). Nevertheless, the young stars in the Galactic center could have an intermediate-mass star origin.

4) Hyper velocity stars (HVSs) are produced by encounters with a cluster of stellar-mass black holes or with the SMBH. Under some restrictions this mechanism could even account for all the B-type HVSs in the halo (O'Leary & Loeb [54] and Kollmeier & Gould [38]). With this in mind, the somewhat exotic solution to the "Paradox of Youth" is suggested by Ginsburg & Loeb [32]. The very high velocities of the S-stars can be seen in Fig. 1.14. The remnants of Hyper Velocity Collisions could create S-stars but it cannot account for all the S-stars in the central parsec.

5) Inspiraling Cluster Scenario (ICS) . A stellar cluster, gravitationally bound to an IMBH, is dragged into the GC. While spiraling in, the majority of the stars get

scattered of. Though this could be a mechanism to account for the S-stars (Portegies Zwart, McMillan & Gerhard [57], Hansen & Milosavljević [34]). However, the inspiraling cluster scenario appears to be in conflict with the observed stellar distribution in the clockwise disk. (Paumerd et al. [56])

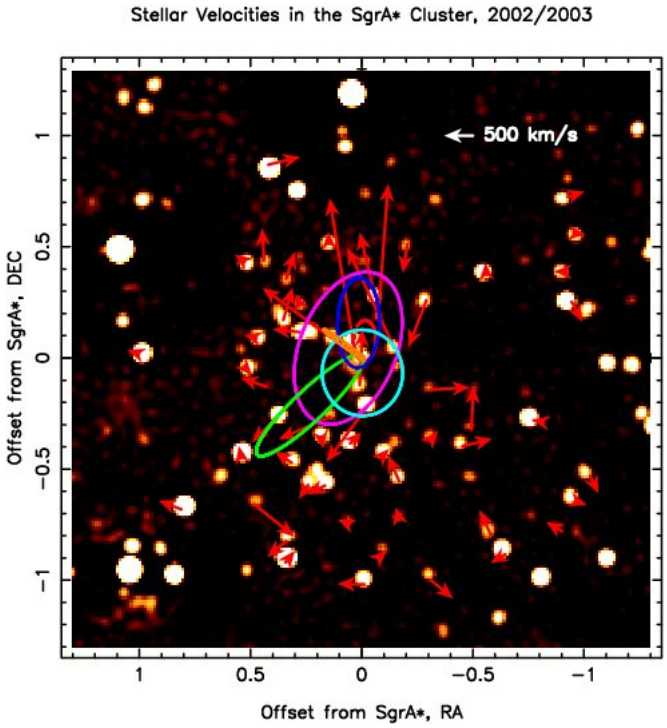

Figure 1.14: The central arcsec

The image above shows a K-band image of the immediate environment of Sgr A* (located at the center). Offsets from Sgr. A* in arcseconds in right ascension and declination are indicated on the axes. The arrows indicate the direction and magnitude of the measured proper motion of the stars within about 1.2" of Sgr A*. A steep increase in the magnitude of the velocities can be seen toward Sgr A*, where velocities exceed several 1000 kms^{-1}. The colored ellipses indicate the orbits as determined for six stars around Sgr A*. The Keplerian orbits give extremely good constraints on the potential and indicate the presence of a point-mass like object (SMBH).

Chapter 2

Modeling proper positions and velocities

2.1 Orbital Parameters

In this chapter we are going to model the orbits of six inner S-stars[1] around the SMBH. In order to do so, we need to find an expression for the positions in space at any arbitrary point in time. This can be done by using the the seven classical orbital parameters: P, a, t_0, e, i, ω and Ω, together with the $Ellipse\ equation$ and the $Kepler\ equation$. For these six S-stars we use the orbital parameters derived by Eisenhauer et al [20].

2.2 Kepler Positions

Let us start with the equation for an ellipse.

$$r = \frac{a(1\ -\ e^2)}{1\ +\ e\cos(\phi)} \tag{2.1}$$

Where a is the $semi\text{-}major\ axis$, e the $eccentricity$ and ϕ is called the $true\ anomaly$.

There is not an analytical way to write the $true\ anomaly\ \phi(t)$ as an explicit function of time. Therefore we use a new coordinate $\mathcal{E}$, known as the $eccentric\ anomaly$ (See Fig. 2.1). Together with the use of $r = a(1 - e\cos(\mathcal{E}))$ and Eq. 2.1 we can find an expression for $\cos(\phi)$:

$$\cos(\phi) = \frac{\cos(\mathcal{E}) - e}{1 - e\cos(\mathcal{E})} \tag{2.2}$$

[1] The six inner S-stars i.e.: S1, S2, S8, S12, S13 & S14

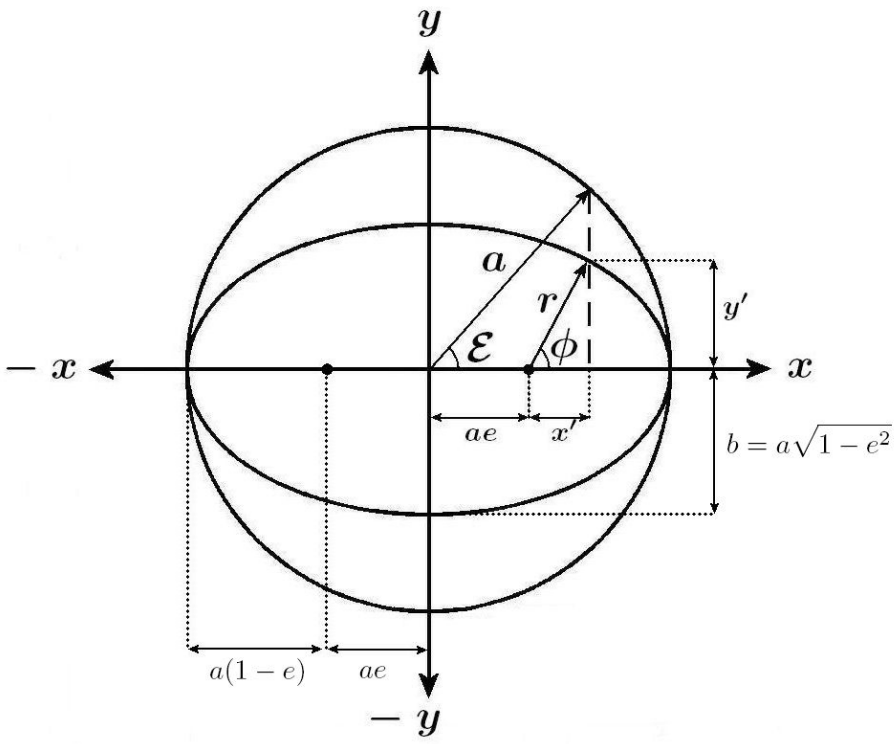

Figure 2.1: Unit Circle versus Ellipse

Unit Circle and Ellipse extended with parameters for Kepler equation. The analogy makes use of: $semi\text{-}major\ axis\ a$, $semi\text{-}minor\ axis\ b$, eccentricity e, eccentric anomaly $\mathcal{E}$, $true\ anomaly\ \phi$ and r the positional vector of the ellipse.

With the use of the second[2] and third[3] law of Kepler, this will lead to the Kepler equation:

$$\mathcal{E} - e\sin(\mathcal{E}) = \frac{2\pi(t-t_0)}{P} \equiv \mathcal{M} \tag{2.3}$$

with t_0 being the $time\ of\ pericenter$ (periastron), P the orbital $period$ and $\mathcal{M}$ is

[2]**Second law of Kepler:** also known as *Law of equal areas*.

$$\frac{dA}{dt} = \frac{1}{2}\sqrt{GMa(1-e^2)}$$

[3]**Third law of Kepler:** also known as *Harmonic Law*.

$$\frac{P^2}{a^3} = \frac{4\pi^2}{GM}$$

known as $mean\ anomaly$.

This needs to be solved numerically, which can be done by the following iterative method:

1. $\mathcal{E}_1 = \mathcal{M},\ i = 1$
2. $\mathcal{E}_{i+1} = \mathcal{M} + e\sin(\mathcal{E}_i)$
3. $i = i + 1$, go to 2

With increasing values of i the solution will become more accurate.

This provides us with a solution for $\mathcal{E}$. Which in its turn, applied to Eq. 2.2, provides us with a solution for $\phi(t)$ and thus the shape of the orbit.

The orientation of the coordinate system we are going to use is equal to the wind-direction system on Earth, as seen from space. Up is North, East to the right, down is South and West is to the left. Besides this we want a reverse x-axis, equal to the equatorial coordinate system. Looking back to Fig. 2.1, the vector r rotates around the center anti-clockwise (prograde), originating from one of the foci on the x-axis. We want the orbit to start from the positive y-axis. Therefore, we substitute the x-axis with the y-axis. Since r originates from the focal point of the ellipse we can describe the positions in time by:

$$x = r\sin(\phi) \tag{2.4}$$

$$y = r\cos(\phi) \tag{2.5}$$

$$z = 0 \tag{2.6}$$

In proceeding with the modeling, we need to make use of the other classical orbital parameters. Note that there is no reason to assume the $semi\text{-}major\ axis$ coexist with one of the axis of orientation. Therefore we need the orbital parameters ω, called $argument\ of\ periastron$. This is the angle between the orbits $semi\text{-}major\ axis$ and our coordinate system's positive y-axis. In other words the ω is the angle of rotation between r at t_0 (periastron) and the positive y-axis (see Fig. 2.2).

$$x = r\sin(\phi + \omega) \tag{2.7}$$

$$y = r\cos(\phi + \omega) \tag{2.8}$$

$$z = 0 \tag{2.9}$$

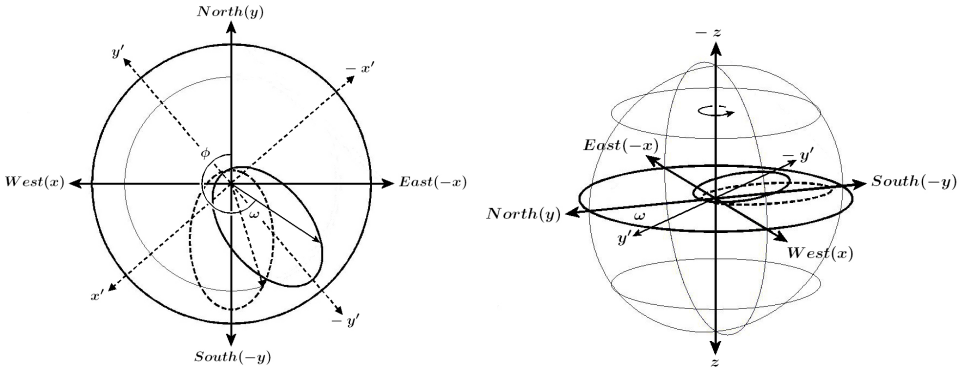

Figure 2.2: Implementation of $argument\ of\ periastron\ \omega$

Left: Projection on plane of the sky. Right: Projection in 3-D model. Dashed ellipse shows the orbit before implementation of $argument\ of\ periastron\ \omega$. The solid line shows the orbit in it's new orientation. The orbit is rotated around the z-axis by an angle ω.

Again there is no reason to assume the orbital plane is equal to the plane of the sky. Therefore we introduce one of the other classical parameters i called the $inclination$. This parameter is used to indicate the rotation, of the orbital plane, around the y-axis compared to the plane of the sky. With reference to Fig. 2.2, if $0° \leqq \omega \leqq 180°$, the West-side of the orbital plane is inclined towards Earth. If $180° \leqq \omega \leqq 360°$, the East-side of the orbital plane is inclined towards Earth.

When we extend our model with i, making it a 3D-model, the positions in our coordinate system can be described as:

$$x = \quad r\sin(\phi+\omega)\cos(i) \tag{2.10}$$

$$y = \quad r\cos(\phi+\omega) \tag{2.11}$$

$$z = -r\sin(\phi+\omega)\sin(i) \tag{2.12}$$

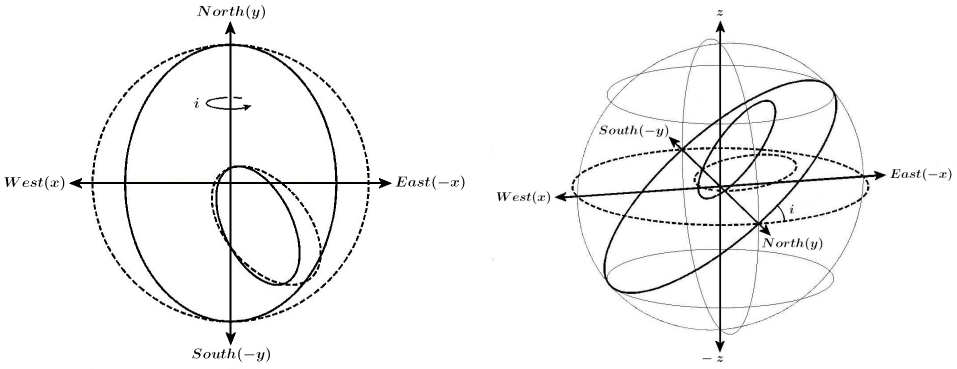

Figure 2.3: Implementation of $inclination\ i$

Left: Projection on plane of the sky. Right: Projection in 3-D model. Dashed line shows the orbit before implementation of $inclination\ i$. The solid line shows the orbit in it's new orientation. The orbit is rotated around the y-axis by an angle i. Note that the orbital plane does not longer coexists with the plane of the sky, making it a true 3-D model.

In order to complete our $3D-$model, we need to include the last classical orbital parameter Ω, known as the $line\ of\ nodes$. The implementation of this parameter can be seen as the rotation of the orbital plane around the z-axis. It is called the line of nodes because this is the line between the two points where the orbit moves through the plane of the sky. Hence, there is one point where the orbit goes through the plane of the sky towards the observer ($descending\ node$). The other point is where the orbit goes through the plane of the sky, away from the observer ($ascending\ node$)[4]. This results in (Kreyszig [40]):,

$$x = x' \cos(-\Omega) \ - \ y' \sin(-\Omega) \tag{2.13}$$

$$y = y' \cos(-\Omega) \ + \ x' \sin(-\Omega) \tag{2.14}$$

$$z = z' \tag{2.15}$$

Where x', y' and z' are the previously obtained x, y and z positions in respectively Eq. 2.10, 2.11 and 2.12. Which leads up to the $proper\ positions$ and Fig. 2.4:

$$x = \quad r \sin(\phi + \omega) \cos(i) \cos(-\Omega) \ - \ r \cos(\phi + \omega) \sin(-\Omega) \tag{2.16}$$

$$y = \quad r \cos(\phi + \omega) \cos(-\Omega) \ + \ r \sin(\phi + \omega) \cos(i) \sin(-\Omega) \tag{2.17}$$

$$z = -\, r \sin(\phi + \omega) \sin(i) \tag{2.18}$$

[4]When Ω lies in the western half of the plane of the sky, and $i \leqq 90^\circ$ the orbit will have a $retrograde$ motion (clockwise). When $\Omega \geqq 180^\circ$ or $i \geqq 90^\circ$ the orbit will have a $prograde$ motion (counterclockwise)

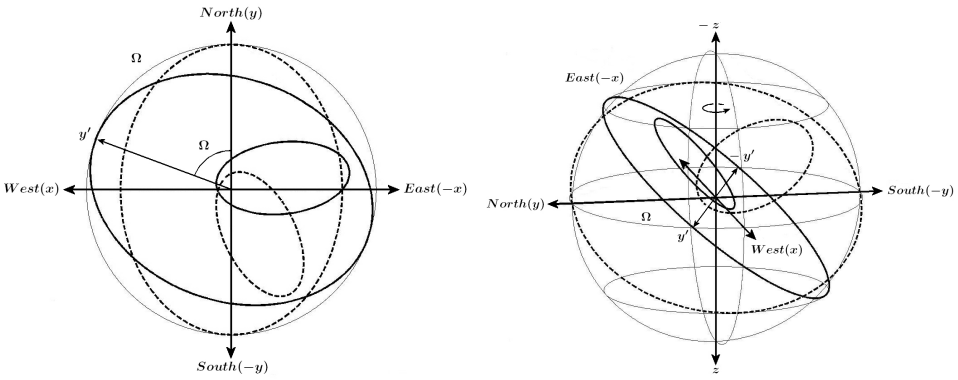

Figure 2.4: Implementation of $line\ of\ nodes\ \Omega$

Left: Projection on plane of the sky. Right: Projection in 3-D model. Dashed line shows the ellipse before implementation of $line\ of\ nodes\ \Omega$. The solid line shows the ellipse in it's new orientation. The ellipse is rotated around the z-axis by an angle Ω. This model is a visualization of an orbit with random classical orbital parameters.

2.2.1 3D-positions of the S-stars

On the previous page we have the expressions for the proper orbital coordinates in the sky. To summarize, the orbital parameters we need: P, a, t_0, e, i, ω and Ω. When talking about a certain orbital parameter of a specific S-star, we will add the name of the S-star as a subscript. For instance, P_{S2} will refer to the orbital period of S2.

We have written a C++ program to generate time-dependent solutions to these equations[5]. With the use of the orbital parameters from Eisenhauer et al. [20] (Table 2.2.1) of the 6 inner S-stars, we can complete our model. Using these values as input for the program, it generates the time-dependent $3D$ positions of the S-stars. The results are plotted in the Fig. 2.5 to 2.7.

[5]For more information on the source code see Appendix B1

parameter/star	S1	S2	S8	S12	S13	S14
alternative name	S0-1	S0-2	S0-4	S0-19	S0-20	S0-16
semi-major axis a	0.412	0.1226	0.329	0.286	0.219	0.225
[arcsec]	(0.024)	(0.0025)	(0.018)	(0.012)	(0.058)	(0.022)
semi-major axis a	3296.0	980.8	2632.0	2288.0	1752.0	1800.0
[AU] [a]	(192.0)	(20.0)	(144.0)	(96.0)	(464.0)	(176.0)
numerical	0.358	0.8760	0.927	0.9020	0.395	0.9389
eccentricity e	(0.036)	(0.0072)	(0.019)	(0.0047)	(0.032)	(0.0078)
orbital period P	94.1	15.24	67.2	54.4	36	38.0
[years]	(9.0)	(0.36)	(5.5)	(3.5)	(15)	(5.7)
epoch of peri-	2002.6	2002.315	1987.71	1995.628	2006.1	2000.156
astron passage t_0	(0.6)	(0.012)	(0.81)	(0.016)	(1.4)	(0.052)
inclination i	120.5	131.9	60.6	32.8	11	97.3
[degrees]	(1.0)	(1.3)	(5.3)	(1.6)	(35)	(2.2)
position angle of	341.5	221.9	141.4	233.3	100	228.5
the ascending node	(0.9)	(1.3)	(1.9)	(4.6)	(198)	(1.7)
Ω [degrees]						
argument of	129.8	62.6	159.2	311.8	250	344.7
periastron ω	(4.7)	(1.4)	(1.8)	(3.6)	(161)	(2.2)
[degrees]						

Table 2.1: The orbital parameters of the six inner S-stars.

From the original publication of Eisenhauer et al. [20]. The values between parentheses are the $\pm 1\sigma$ uncertainties and include an uncertainty of $\pm 0.32\,kpc$ in $R_0 = 8.0\,kpc$. Central mass (CM): $M_{CM} = M_0 = 4.06 \pm 0.38 \cdot 10^6\,M_\odot$.

[a] These are the converted values of the $semi\text{-}major\ axis$ in $arcsec$ to AU.

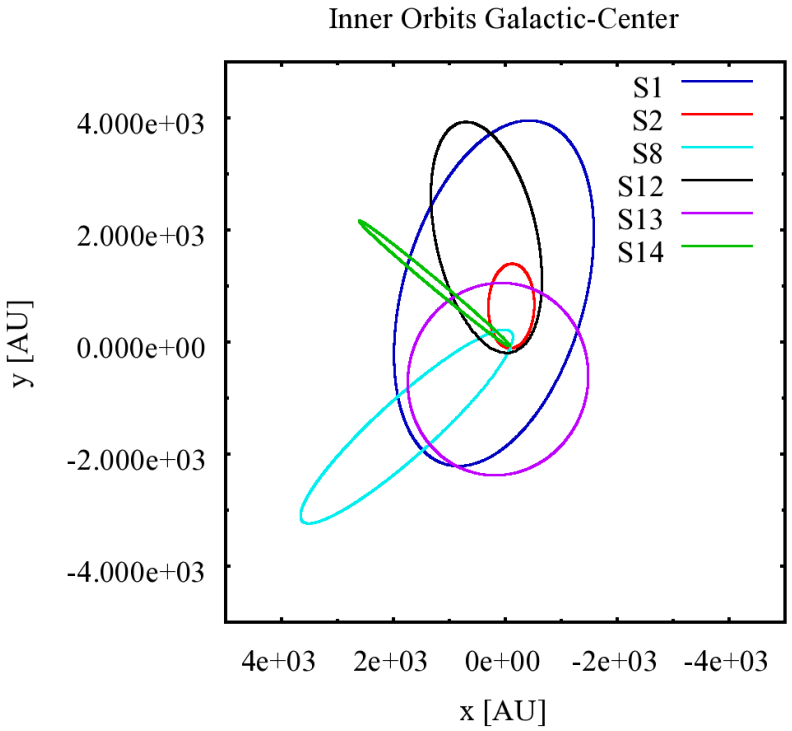

Figure 2.5: The Orbits of the inner 6 S-stars in x, y-projection

The x, y-projection of the positions of the six 6 inner S-stars, using the orbital parameters P, a, t_0, e, i, ω and Ω, of the original publication of Eisenhauer et al. [20]. The positions of the S-stars: S1, S2, S8, S12, S13, S14; are plotted for $t = 2000 + P_{S0-1}\, yrs$ with $P_{S0-1} = 94.1\, yrs$ and a time-step $dt = 0.1825\, yrs$.

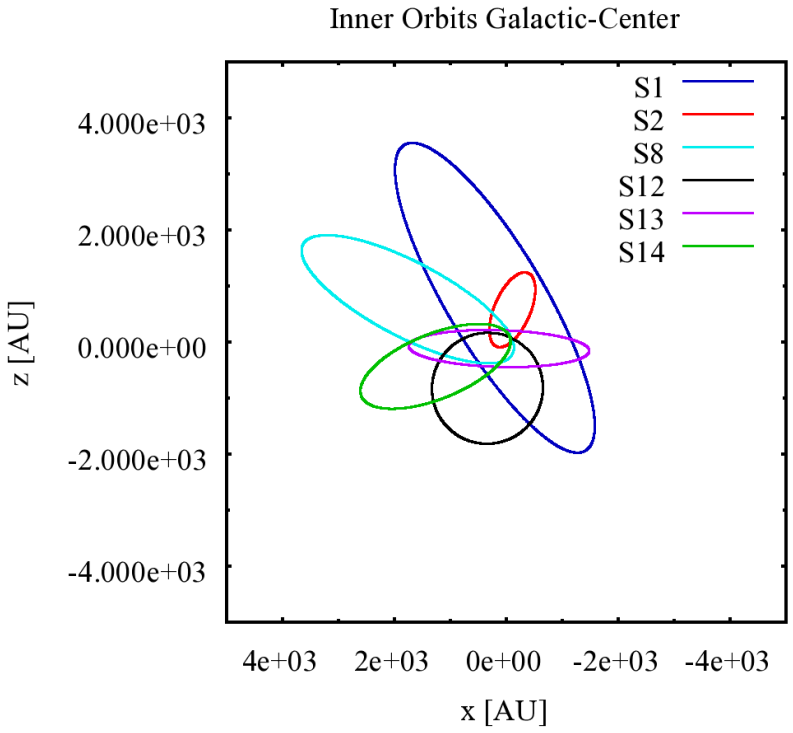

Figure 2.6: The Orbits of the inner 6 S-stars in x, z-projection

The x, z-projection of the positions of the six 6 inner S-stars, using the orbital parameters P, a, t_0, e, i, ω and Ω, of the original publication of Eisenhauer et al. [20]. The positions of the S-stars: S1, S2, S8, S12, S13, S14; are plotted for $t = 2000 + P_{S0-1}\, yrs$ with $P_{S0-1} = 94.1\, yrs$ and a time-step $dt = 0.1825\, yrs$.

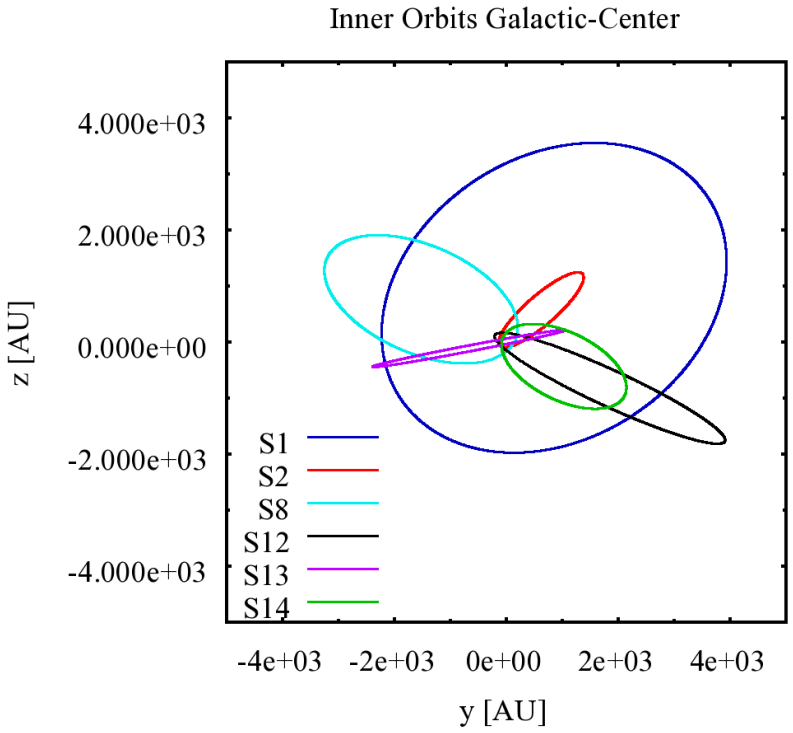

Figure 2.7: The Orbits of the inner 6 S-stars in y, z-projection

The y, z-projection of the positions of the six 6 inner S-stars, using the orbital parameters P, a, t_0, e, i, ω and Ω, of the original publication of Eisenhauer et al. [20]. The positions of the S-stars: S1, S2, S8, S12, S13, S14; are plotted for $t = 2000 + P_{S0-1}\, yrs$ with $P_{S0-1} = 94.1\, yrs$ and a time-step $dt = 0.1825\, yrs$.

2.3 Kepler Velocities

In the previous section we derived expressions for the Galactic x, y and z positions with the use of the $Kepler$ and $ellipse\ equation$. In this section we will derive the expressions for the velocities.

Since $v_x = \dot{x}$, $v_y = \dot{y}$ and $v_z = \dot{z}$, we get the following:

$$\begin{aligned} v_x &= r\dot{\phi}\cos(\phi+\omega)\cos(i)\cos(-\Omega) + \dot{r}\sin(\phi+\omega) \\ &\quad + r\dot{\phi}\sin(\phi+\omega)\sin(-\Omega) - \dot{r}\cos(\phi+\omega)\sin(-\Omega) \end{aligned} \tag{2.19}$$

$$\begin{aligned} v_y &= -r\dot{\phi}\sin(\phi+\omega)\cos(-\Omega) + \dot{r}\cos(\phi+\omega)\cos(-\Omega) \\ &\quad + r\dot{\phi}\cos(\phi+\omega)\cos(i)\sin(-\Omega) + \dot{r}\sin(\phi+\omega)\cos(i)\sin(-\Omega) \end{aligned} \tag{2.20}$$

$$v_z = -r\dot{\phi}\cos(\phi+\omega)\sin(i) - \dot{r}\sin(\phi+\omega)\sin(i) \tag{2.21}$$

With the use of the following expressions we can rewrite the derivatives.

$$\begin{aligned} & r\dot{\phi} = \frac{J}{mr} \quad \text{and} \quad \dot{r} = \frac{er\dot{\phi}\sin(\phi)}{1+\cos(\phi)} = \frac{eJ}{mr}\frac{\sin(\phi)}{(1+\cos(\phi))} \\ & \text{with} \quad \frac{J}{m} = \frac{2\pi}{P}\,a^2\sqrt{1-e^2} \quad \text{and} \quad r = \frac{a(1-e^2)}{1+e\cos\phi} \\ & \text{Gives} \quad \frac{J}{mr} = \frac{2\pi}{P}\,a^2\sqrt{1-e^2}\,\frac{1+e\cos\phi}{a(1-e^2)} = \frac{2\pi}{P}\,\frac{a(1+e\cos\phi)}{\sqrt{1-e^2}} \\ & \text{So} \quad r\dot{\phi} = \frac{2\pi}{P}\,\frac{a(1+e\cos\phi)}{\sqrt{1-e^2}} \quad \text{and} \quad \dot{r} = \frac{2\pi}{P}\,\frac{ae\sin\phi}{\sqrt{1-e^2}} \end{aligned} \tag{2.22}$$

This will lead to:

$$\begin{aligned} v_x &= \frac{2\pi}{P}\,\frac{a(1+e\cos(\phi))}{\sqrt{1-e^2}}\left[\,\cos(\phi+\omega)\cos(i)\cos(-\Omega)\,\right] \\ &\quad + \frac{2\pi}{P}\,\frac{ae\sin(\phi)}{\sqrt{1-e^2}}\left[\,\sin(\phi+\omega)\cos(i)\cos(-\Omega)\,\right] \\ &\quad + \frac{2\pi}{P}\,\frac{a(1+e\cos(\phi)}{\sqrt{1-e^2}}\left[\,\sin(\phi+\omega)\sin(-\Omega)\,\right] \\ &\quad - \frac{2\pi}{P}\,\frac{ae\sin(\phi)}{\sqrt{1-e^2}}\left[\,\cos(\phi+\omega)\sin(-\Omega)\,\right] \end{aligned}$$

$$
\begin{aligned}
v_y &= -\frac{2\pi}{P}\frac{a(1+e\cos(\phi))}{\sqrt{1-e^2}}\left[\,\sin(\phi+\omega)\cos(-\Omega)\,\right] \\
&\quad +\frac{2\pi}{P}\frac{ae\sin(\phi)}{\sqrt{1-e^2}}\left[\,\cos(\phi+\omega)\cos(-\Omega)\,\right] \\
&\quad +\frac{2\pi}{P}\frac{a(1+e\cos(\phi))}{\sqrt{1-e^2}}\left[\,\cos(\phi+\omega)\cos(i)\sin(-\Omega)\,\right] \\
&\quad -\frac{2\pi}{P}\frac{ae\sin(\phi)}{\sqrt{1-e^2}}\left[\,\sin(\phi+\omega)\cos(i)\sin(-\Omega)\,\right]
\end{aligned}
$$

$$
\begin{aligned}
v_z &= \frac{2\pi}{P}\frac{a(1+e\cos(\phi))}{\sqrt{1-e^2}}\left[\,\cos(\phi+\omega)\sin(i)\,\right] \\
&\quad -\frac{2\pi}{P}\frac{ae\sin(\phi)}{\sqrt{1-e^2}}\left[\,\sin(\phi+\omega)\sin(i)\,\right]
\end{aligned}
$$

Rearranging and making use of the law of cosine [6] we write the rather cumbersome notation of the proper velocities in it's final form:

$$
\begin{aligned}
v_x &= K\,\cos(i)\,\cos(-\Omega)\left[\,cos(\phi+\omega)\,+\,e\cos(\omega)\right] \\
&\quad +K\,\sin(-\Omega)\left[\,\sin(\phi+\omega)\,-\,e\sin(\omega)\,\right]
\end{aligned}
\tag{2.23}
$$

$$
\begin{aligned}
v_y &= K\,\cos(i)\,\sin(-\Omega)\left[\,\cos(\phi+\omega)\,+\,e\cos(\omega)\right] \\
&\quad -K\,\cos(-\Omega)\left[\,\sin(\phi+\omega)\,-\,e\sin(\omega)\,\right]
\end{aligned}
\tag{2.24}
$$

$$
v_z = -K\,\sin(i)\left[\,\cos(\phi+\omega)\,+\,e\cos(\omega)\right] \tag{2.25}
$$

$$
\text{with}\quad K=\frac{2\pi}{P}\frac{a}{\sqrt{1-e^2}}
$$

[6] **Law of cosine:**

$$
\begin{aligned}
\cos(\alpha-\beta) &= \cos(\alpha)cos(\beta)+\sin(\alpha)\sin(\beta) \\
&\quad \text{with}\quad \alpha=\phi+\omega\,,\beta=\phi \\
\sin(\alpha-\beta) &= \sin(\alpha)cos(\beta)-\sin(\beta)\cos(\alpha) \\
&\quad \text{with}\quad \alpha=\phi+\omega\,,\beta=\phi
\end{aligned}
$$

2.3.1 3D-velocities of the S-stars

These expressions are also implemented in the earlier mentioned C++ program. Using the solutions from the code and visualizing them, we get Fig. 2.8 to 2.10. Note that due to the very high velocities of these S-stars, the plotted orbits are not fully elliptic. Together with orbit overlap, for the orbits of the stars with $P < P_{S0-1}$, there can be some irregularities in the plotting of their velocities.

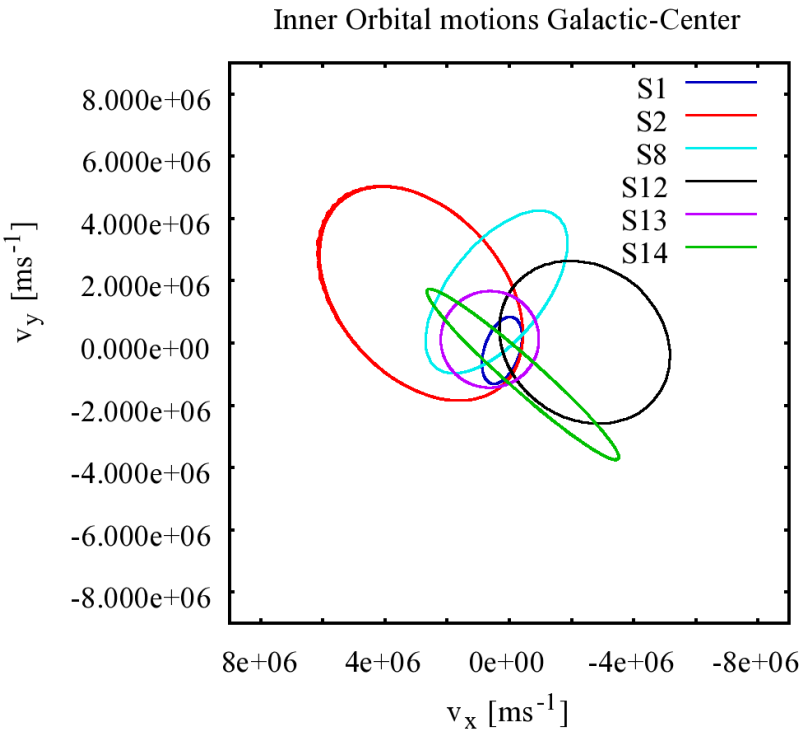

Figure 2.8: The orbital velocities of the inner 6 S-stars in v_x,v_y-projection

The x, y-projection of the velocities of the six 6 inner S-stars, using the orbital parameters P, a, t_0, e, i, ω and Ω, of the original publication of Eisenhauer et al. [20]. The velocities of the S-stars: S1, S2, S8, S12, S13, S14; are plotted for $t = 2000 + P_{S1}\, yrs$, with $P_{S1} = 94.1\, yrs$ and a time-step $dt = 0.1825\, yrs$. This results in some overlap for the orbits of the stars with $P < P_{S1}$, emphasizing the high velocities of these S-stars

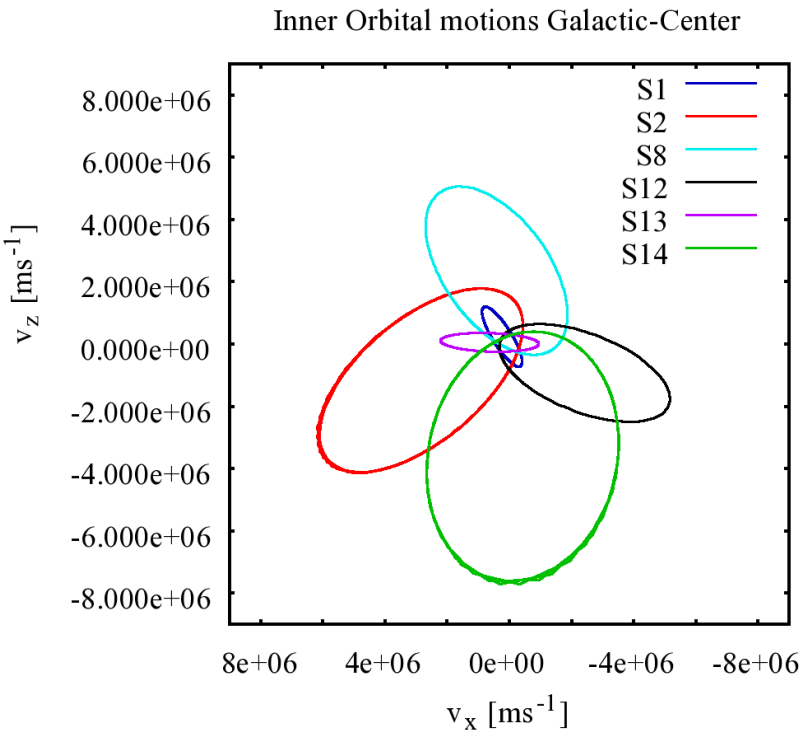

Figure 2.9: The orbital velocities of the inner 6 S-stars in v_x,v_z-projection

The x, z-projection of the velocities of the six 6 inner S-stars, using the orbital parameters P, a, t_0, e, i, ω and Ω, of the original publication of Eisenhauer et al. [20]. The velocities of the S-stars: S1, S2, S8, S12, S13, S14; are plotted for $t = 2000 + P_{S1}\, yrs$, with $P_{S1} = 94.1\, yrs$ and a time-step $dt = 0.1825\, yrs$. This results in some overlap for the orbits of the stars with $P < P_{S1}$, emphasizing the high velocities of these S-stars

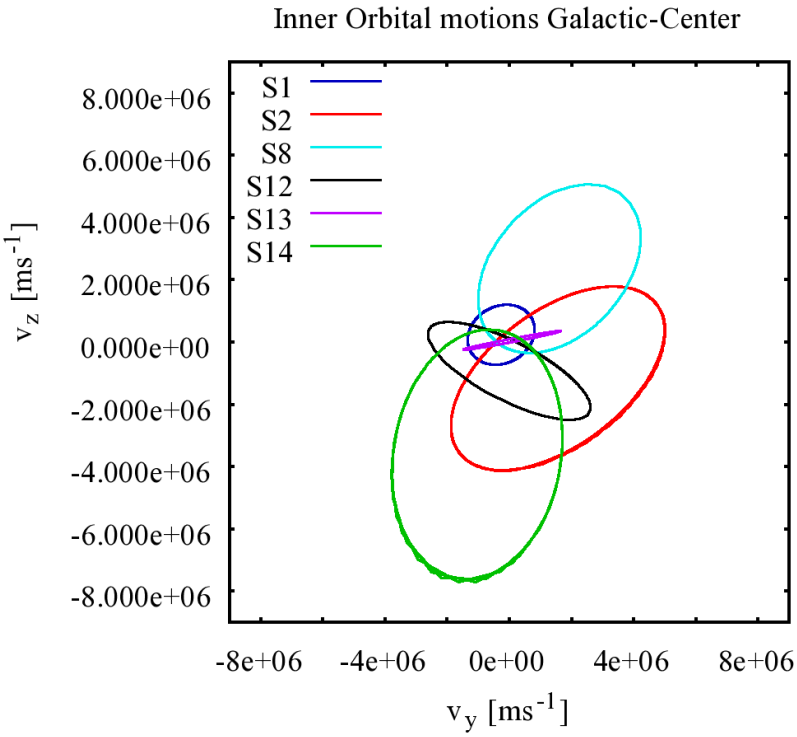

Figure 2.10: The orbital velocities of the inner 6 S-stars in v_y,v_z-projection

The y, z-projection of the velocities of the six 6 inner S-stars, using the orbital parameters P, a, t_0, e, i, ω and Ω, of the original publication of Eisenhauer et al. [20]. The velocities of the S-stars: S1, S2, S8, S12, S13, S14; are plotted for $t = 2000 + P_{S1}\, yrs$, with $P_{S1} = 94.1\, yrs$ and a time-step $dt = 0.1825\, yrs$. This results in some overlap for the orbits of the stars with $P < P_{S1}$, emphasizing the high velocities of these S-stars

Chapter 3

N-body based Solution to the Positions of the S-stars

In the previous chapter, we have constructed the orbits without interaction between the individual S-stars. This 'system of binaries' is based on the assumption that the orbits, of the S-stars, are totally dominated by the gravitational pull of the $\pm 4.06 \times 10^6$ $M_\odot$ of the SMBH associated with Sgr. A* (Ghez et al. [29], Ghez et al. [30] and Eisenhauer et al. [20]). In this chapter, we are going to present a joint solution of the orbits (i.e. the six S-stars + SMBH). This will be done by means of symplectic integration with a N-body code called HNBody from Rauch & Hamilton [61]. With this N-body code we explore the stability and time evolution of the joint '7-body' system.

3.1 Basics of N-body Systems

Consider a system of N particles in virial equilibrium. Originating from Heggie & Mathieu [35], with $G = M = 1$ and $E = -\frac{1}{4}$, which leads to $r_V = 1$. With the virial radius r_V being the inverse of the average inverse distance between particles in the system. Or, in the words of Heggie & Mathieu [35], the harmonic mean particle separation.

$$\frac{1}{r_V} = \left\langle \sum_{i \neq j} \frac{1}{|\mathbf{r}_i - \mathbf{r}_j|} \right\rangle \tag{3.1}$$

So for a general system of particles with masses m_i and total mass M:

$$\frac{M^2}{r_V} = \sum_i \sum_{j,j \neq i} \frac{m_i\, m_j}{|\mathbf{r}_i - \mathbf{r}_j|} \tag{3.2}$$

Which equals twice the potential energy of an N-body system, with $G = 1$.

This results in:

$$E_{pot} = -G \sum_{i<j} \frac{m_i\, m_j}{|\mathbf{r}_i - \mathbf{r}_j|} = -\frac{1}{2}\frac{GM^2}{r_V} \tag{3.3}$$

With the use of the virial theorem[1], this results in:

$$E_{tot} = \frac{1}{2}E_{pot} = -\frac{1}{4}\frac{GM^2}{r_V}, \text{ with } G = M = 1,\ E_{tot} = -\frac{1}{4}\frac{1}{r_V} \tag{3.4}$$

With the associated units (Heggie and Mathieu [35]):

$$U_{\text{mass}} = M, \qquad U_{\text{length}} = -\frac{GM^2}{4E} \quad \text{and} \quad U_{\text{time}} = \frac{GM^{\frac{5}{2}}}{(-4E)^{\frac{3}{2}}}$$

As a consequence, dynamical calculations of N-body systems will result in G, M and E or r_V dependent solutions. Since these variables are chosen to be equal to 1, it is easy to make errors, during calculations, when working with these dimensionless variables. One of the main advantages of the HNBody-code is that it can produce results in a variety of astrophysical units, without having to worry about this conversion of units. With this in mind, we have decided to use the HNBody-code for our evaluation of the Sgr. A* star cluster.

3.2 HNBody

3.2.1 Symplectic Integration

Besides not having to worry about units, there is another good reason for using the HNBody package. The code provides the possibility of symplectic integration. Symplectic integration schemes are highly efficient and provide long-term stability of dynamical systems. It is based on conservation of the Hamiltonian 2-form $dp \wedge dq$, with (q, p) being the canonical phase-space coordinates, which is known as a symplectic 2-form. This results in the preservation of (Saha & Tremaine [66])phase-space area for a two-dimensional phase space (Duncan, Levison & Lee

[1] **Virial Theorem**: The earliest clear presentation of the virial theorem was presented by Claussius on June 13, 1870. It states, in contemporary language of energy, the average kinetic energy is equal to 1/2 the average potential energy. So for a system with a total average kinetic energy $\langle T \rangle$ and its average total potential energy $\langle V_{Tot} \rangle$, the virial theorem states: $2\langle T \rangle = -\sum_{k=1}^{N} \langle \mathbf{F}_k \cdot \mathbf{r}_k \rangle$, where $\mathbf{F}_k$ represents the force on the kth particle, which is located at position $\mathbf{r}_k$ (G. W. Collins, II 1978 [12]).

[16]). Consequently, placing tight constraints on the global geometry of the dynamics (Channell & Scovel [8], Quinn et al. [59]).

As a reminder, Hamilton's equations read:

$$\dot{p} = -\frac{\partial H}{\partial q} \text{ and } \dot{q} = \frac{\partial H}{\partial p} \tag{3.5}$$

with H being the Hamiltonian.

Because most symplectic integrators, like the HNBody symplectic integrator, are based on splitting methods. Consider a separable Hamiltonian:

$$H(p, q) = T(p) + V(q) \tag{3.6}$$

with T the kinetic energy and V the potential energy.

This results in the equations of motion:

$$\dot{z} = \{z, H(z)\} \tag{3.7}$$

With $\{\cdot, \cdot\}$ being a Poisson bracket and using $D_H = \{\cdot, H\}$, we can rewrite this into:

$$\dot{z} = D_H z \tag{3.8}$$

This leads to the solution:

$$z(\tau) = e^{\tau D_H} z(0) \tag{3.9}$$

with τ being the time-step. This gives in combination with Eq. 3.5:

$$z(\tau) = e^{\tau (D_T + D_V)} z(0) \tag{3.10}$$

The time-evolution operator $e^{\tau (D_T + D_V)}$ is approximated by:

$$e^{\tau (D_T + D_V)} = \Pi_{i=1}^{k} e^{c_i \tau D_T} e^{d_i \tau D_V} + O(\tau^{k+1}) \tag{3.11}$$

with c_i and d_i being real numbers and k the order of the integration (Saha & Tremaine [66]).

This results in respectively $e^{c_i \tau D_T}$, $e^{d_i \tau D_V}$ mapping:

$$\begin{pmatrix} q \\ p \end{pmatrix} \mapsto \begin{pmatrix} q' \\ p' \end{pmatrix} = \begin{pmatrix} q + \tau c_i \frac{\partial T}{\partial p}(p) \\ p \end{pmatrix} , \begin{pmatrix} q \\ p \end{pmatrix} \mapsto \begin{pmatrix} q' \\ p' \end{pmatrix} = \begin{pmatrix} q \\ p - \tau d_i \frac{\partial V}{\partial q}(q) \end{pmatrix} .$$

The coefficients, c_i and d_i, can be determined by the Baker-Campbell-Hausdorff (BCH) formula (Yoshida [76]).

Forest & Ruth [23] have stated: a fourth order integration step preserves exactly the canonical character of the equations of motion. Together with the possibility of setting the HNBody code to a fourth order symplectic integration, we present the values for the coefficients:

$$c_1 = c_4 = \frac{1}{2(2 - 2^{1/3})} , c_2 = c_3 = \frac{1 - 2^{1/3}}{2(2 - 2^{1/3})}$$

$$d_1 = d_3 = \frac{1}{2 - 2^{1/3}} , d_2 = -\frac{2^{1/3}}{2 - 2^{1/3}} , d_4 = 0$$

3.2.2 HNBody Input Parameters

In order to use the HNBody code we have to set the parameters of the code[2] to the right initial values. We need to set the *integration properties*, *properties of the initial conditions* and the *initial conditions* in the input file. In the *integration properties*, see below, we set the values of the integrator (symplectic), the order of integration (fourth), the integration coordinate system (Barycentric) and the corrector (true):

```
# INTEGRATION PROPERTIES

Integrator: Symplectic
#  choices are: Symplectic [Default], Burlisch-Stoer, Runge-Kutta
#  for B-S and R-K there is an optional second value, the accuracy to use
#                                                     (default: 1e-12)
#
# The following three options are meaningful only with Symplectic integrations;
# they specify the canonical coordinates and splitting to use, whether to
# utilize a symplectic corrector, and whether to follow close encounters:
#
IntegCoord: Jacobi Order4
#Order4 Shift-Drift
#IntegCoord: RegJacobi Order4 Shift-Drift
#  primary   values are: Jacobi (or Barycentric) [Default],
#  RegJacobi (or RegBarycentric), Bodycentric
#  secondary values are: Order2 [Default], Order4
#  tertiary  values are: Kick-Drift [Default], Drift-Kick, Shift-Drift
#
```

[2]The HNBody comes with an elaborate sample file called sample.hnb which can be found in Appendix B.2

```
Corrector: true
#  choices are: false/no [Default], true/yes, Order2, Order4, Order6
#               (true or yes means to use the highest available order)
```

In the *properties of initial conditions*, see below, we define the units we want to use (degrees, AU, $M_\odot$ & years), the stepsize of the integrator (0.001 years), mass of the dominant object (4.06×10^6 $M_\odot$) and the number of objects (7):

```
# PROPERTIES OF INITIAL CONDITIONS

AngleUnit:  deg # base unit choices: deg, rad
LengthUnit: AU # base unit choices: m, AU (or ua), pc
MassUnit:   Msun   # 2e27 kg # base unit choices: g, Msun
TimeUnit:   yr  # base unit choices: s, h, d, yr
StepSize:   0.001  # integration time step       (units of TimeUnit)
M  =  4.06e6 # mass of the dominant object (units of MassUnit)
N  =  7  # number of objects (including the dominant mass)

#OblateJ2 = 0 # J2 parameter of dominant mass (default is 0).
#OblateRadius = 0 # J2 radius    of dominant mass (default is 0).
PostNewtonian: yes # Include leading-order post-Newtonian corrections?
#   (default is false/no)
```

The 7 objects in the *properties of initial conditions* consist out of the six S-stars together with the SMBH. Each object requires seven parameters, i.e. mass and six independent phase space coordinates. The most common combination to use is the astrometric positions together with the velocities and the mass. We have chosen to take a combination of orbital parameters as close as possible to the original work from Eisenhauer et al. [20] as enclosed in Table 2.2.1. The HNBody code accepts these orbital parameters as viable input with three minor adjustments: 1) The *line of nodes* originates in the HNBody code from the x-axis instead of the y-axis (longitude of the ascending node). Therefore we added 90 degrees to this value in order to get the orbits in the right angular position. 2) The second adjustment is adding the mass of the S-stars, currently estimated to be ~ 15 M_0 (Morris & Nayakshin[50]). 3) The third adjustment is changing the *time of pericenter* to the *mean anomaly*

This results into the set of initial conditions as input for the HNBody code as seen below.

```
# INITIAL CONDITIONS

Mass  SemiMajorAxis  Ecc  Incl  LongAscendNode  ArgPeriapse  MeanAnomaly
15    3296.0        0.358     120.5     71.5       129.8      -9.946865038
15    980.8         0.87600   131.9     311.9      62.6       -54.68503938
15    2632.0        0.92700   60.6      231.4      159.2      24.58
15    2288.0        0.90200   32.8      323.3      311.8      28.93235294
15    1752.0        0.39500   11        190        250        -61
15    1800.0        0.93890   97.3      318.5      344.7      -1.476
```

This makes the HNBody code initialize with the right settings and input-parameters. You have maybe wondered about why we changed the *time of pericenter* to *mean anomaly* while the sample.hnb file (Appendix B.2) suggests *time of periastron* as a legitimate input parameter. This adjustment is a result from the first evaluations of the HNBody code, which we will discuss in the next subsection.

3.2.3 Evolution of Individual S-star Orbits

Before we evaluate the joint 7-body system, we check the solutions of all the 'binary', S-star - SMBH, configurations. We start this by setting the number of objects $N = 2$, in the *properties of initial conditions*. Together with commenting all but the to be evaluated S-star in the *initial conditions*. In order to check the stability of the code and the evolution of a system in a particular configuration, we keep track of variations in the solution of three orbital parameters of the S-stars: the *semi-major axis*, *eccentricity* and *inclination*. If the code or the system is unstable, the time-dependent solutions of these three independent phase space coordinates will show anomalies. Therefore we set the parameters of HNBody to evolve the "binary-systems" over the period -10^3 to $+10^3$ yrs. The results of these calculations are presented in Table. 3.1 on the pages 40-41.

In contrast with all the positive properties of using HNBody, there is a downside. The HNBody code loses its strength when evaluating close encounters. This is a known weakness of the symplectic integrator (Rauch & Hamilton[61]). Although, we did not expect close encounters to occur, it seems that the extreme mass ratios together with high eccentricity and velocities of the S-stars, generates a similar effect. We have noticed the occurrence of 'spikes', in the solutions, for the S-stars with high eccentricities (e.g. S2, see Table. 3.1). Referring to the last remark of the previous subsection, when running the code with the input-parameter *time of pericenter*, instead of *mean anomaly*, it became clear that these spikes all occurred at t_0. Replacing the *time of pericenter* with the *mean anomaly*, caused the spikes to occur at $t_{pericenter}$ for the involved S-star. As shown, this did not remove these features from the solutions but it is responsible for the correct time-alignment of the orbits. In order to be sure this feature is not time-step related we calculate the parameters over these anomalies with a time-step of only 10^{-7} yr. This results in equal solutions as shown in Table. 3.1. Having tried various other combinations of input parameters did also not result in solutions without the spikes. Therefore, we assume these spikes are an artifact of the HNBody code.

The accuracy of the solutions over a -10^3 to $+10^3$ yrs period is better compared to the accuracy of the initial values. The solution of the *semi-major axis* of S2 has a standard deviation of $\pm 1\sigma = 2.51$ AU , which is a factor $\pm 2.5 \times 10^{-3}$ of its initial value. Although the orbit of S2 has the most accurate values for its orbital parameters, the uncertainty in the observational value presented by Eisenhauer et

al. [20] is almost ten times bigger compared to the mean value of the solution from the HNBody code.

As a verification, we have also investigate the influence of the S2 spikes on the energy error in its 2-body configuration. The resulting energy fluctuations in this configuration has a maximum factor of 6×10^{-13} (See Fig. 3.1). The mean value of 9.36×10^{-16} with $\pm 1\sigma = 2.15 \times 10^{-14}$, is very small compared to the uncertainties in the initial value of the orbital parameters, See Table 2.2.1, which are of an order $\sim 10^{-2}$ for S2. In the case of the inclination value of S13, the uncertainty is even of the same order. We conclude that although the earlier mentioned peaks are seen in the figures of S2, S8, S12 and S14, the HNBody code can be considered stable and provides accurate solutions in terms of relative energy errors.

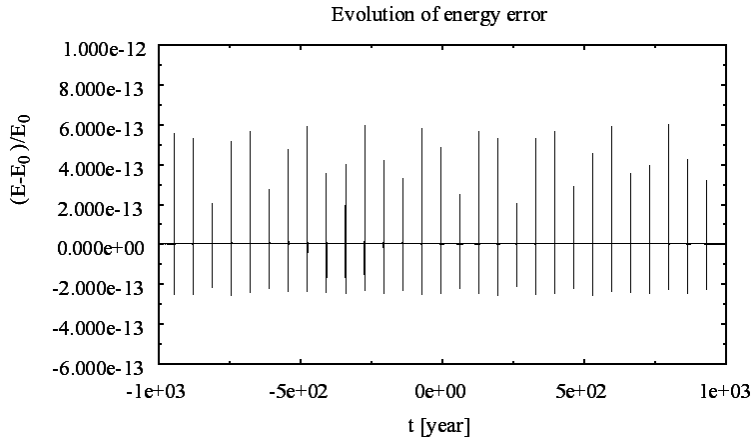

Figure 3.1: The error in system energy

The error in the energy of the system S2 + SMBH for the period -10^3 to $+10^3$ yrs and $dt = 0.1\,yrs$, using the orbital parameters P, a, t_0, e, i, ω and Ω, from Eisenhauer et al. [20]. The mean value is 9.36×10^{-16} with $\pm 1\sigma = 2.15 \times 10^{-14}$.

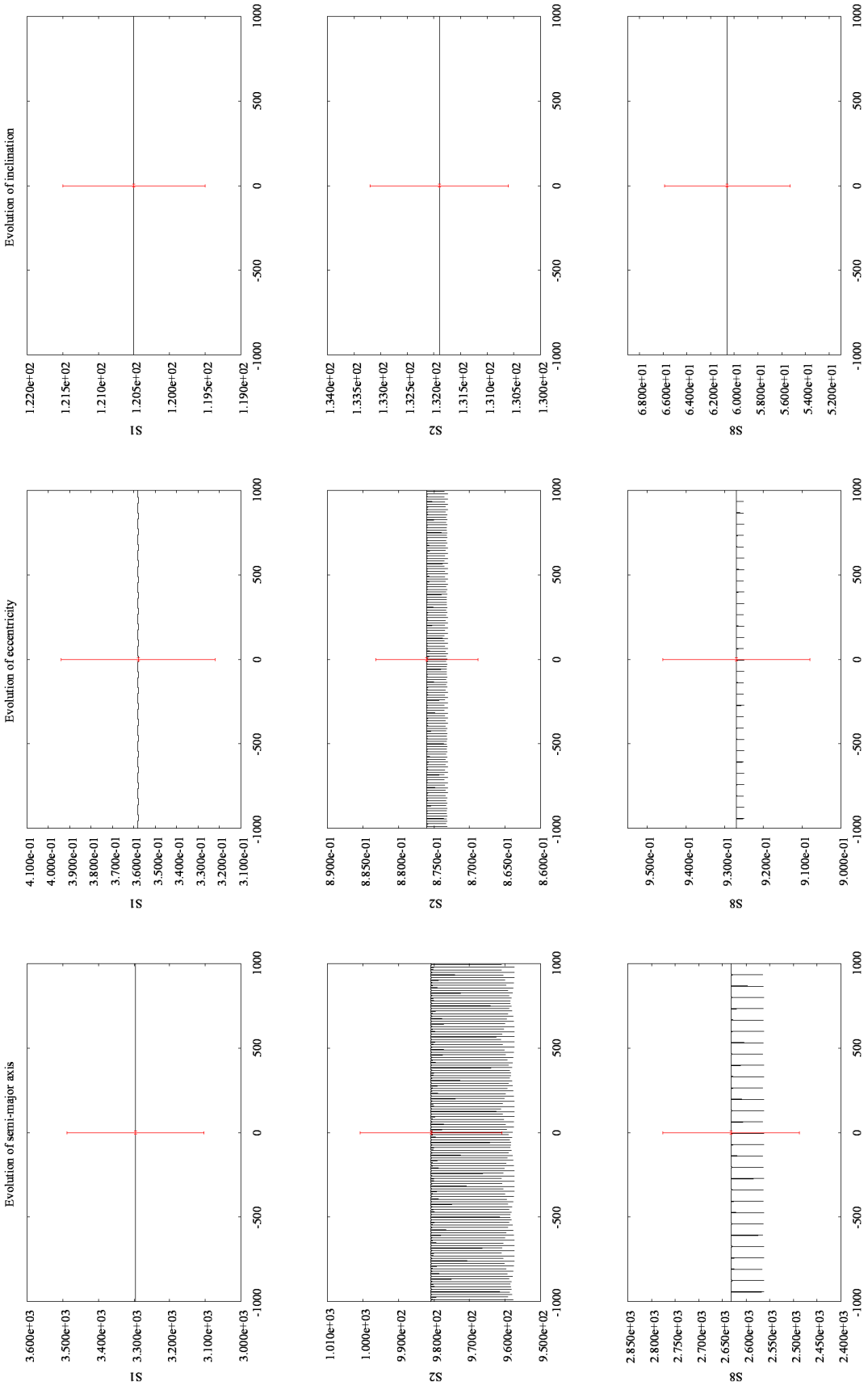
Evolution of inclination
Evolution of eccentricity
Evolution of semi-major axis
S1
S2
S8
1.220e+02
1.215e+02
1.210e+02
1.205e+02
1.200e+02
1.195e+02
1.190e+02
1.340e+02
1.335e+02
1.330e+02
1.325e+02
1.320e+02
1.315e+02
1.310e+02
1.305e+02
1.300e+02
6.800e+01
6.600e+01
6.400e+01
6.200e+01
6.000e+01
5.800e+01
5.600e+01
5.400e+01
5.200e+01
4.100e-01
4.000e-01
3.900e-01
3.800e-01
3.700e-01
3.600e-01
3.500e-01
3.400e-01
3.300e-01
3.200e-01
3.100e-01
8.900e-01
8.850e-01
8.800e-01
8.750e-01
8.700e-01
8.650e-01
8.600e-01
9.500e-01
9.400e-01
9.300e-01
9.200e-01
9.100e-01
9.000e-01
3.600e+03
3.500e+03
3.400e+03
3.300e+03
3.200e+03
3.100e+03
3.000e+03
1.010e+03
1.000e+03
9.900e+02
9.800e+02
9.700e+02
9.600e+02
9.500e+02
2.850e+03
2.800e+03
2.750e+03
2.700e+03
2.650e+03
2.600e+03
2.550e+03
2.500e+03
2.450e+03
2.400e+03
-1000
-500
0
500
1000

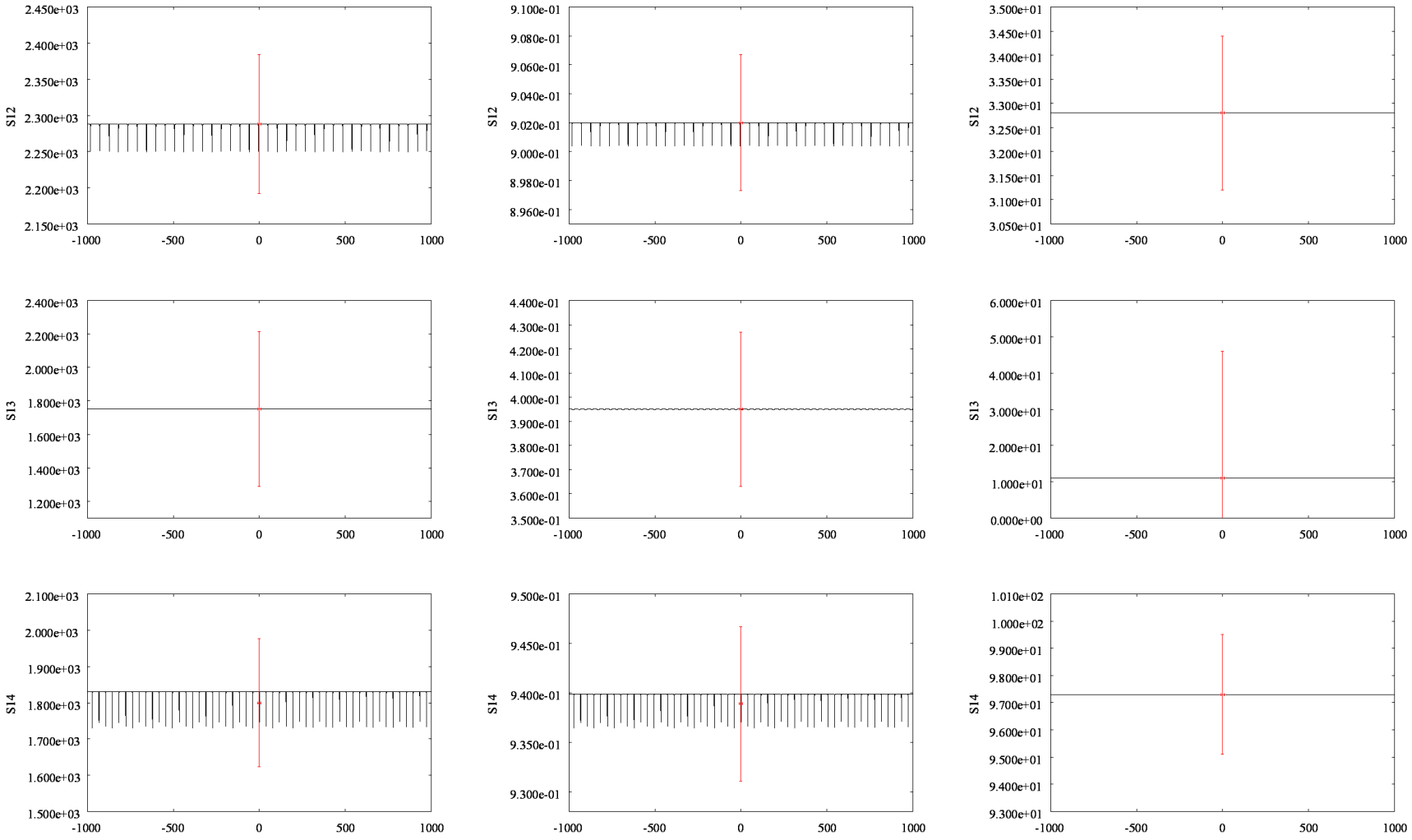

Table 3.1: The evolution of *semi-major axis*, *eccentricity* and *inclination* of the six inner 'S'-stars.

The evolution of *semi-major axis*, *eccentricity* and *inclination* of the six inner 'S'-stars (i.e. S1, S2, S8, S12, S13 & S14) in the 6 binary configurations (i.e. 6 isolated solutions). The solutions of the orbital parameters are plotted for the period that ranges from -10^3 to $+10^3$ yrs, with $t_0 = 2000$ yr. Initial values are taken from Eisenhauer et al. [20]. Note. The peaks occurring at $t_{pericenter}$ in the solutions, are due to artifacts of the HNBody code. The maximum deviation from its mean value, in the *semi-major axis* of S2 is $\pm 1\sigma = 2.51$ AU, which is a factor $\pm 2.5 \times 10^{-3}$ of its initial value.

As a comparison to the orbits presented by Eisenhauer et al. [20][Chapter 1, 1.13] and the solutions obtained with the *Kepler* code from [Chapter 2, 2.5], we have plotted the positions obtained with HNBody in Fig. 3.2.

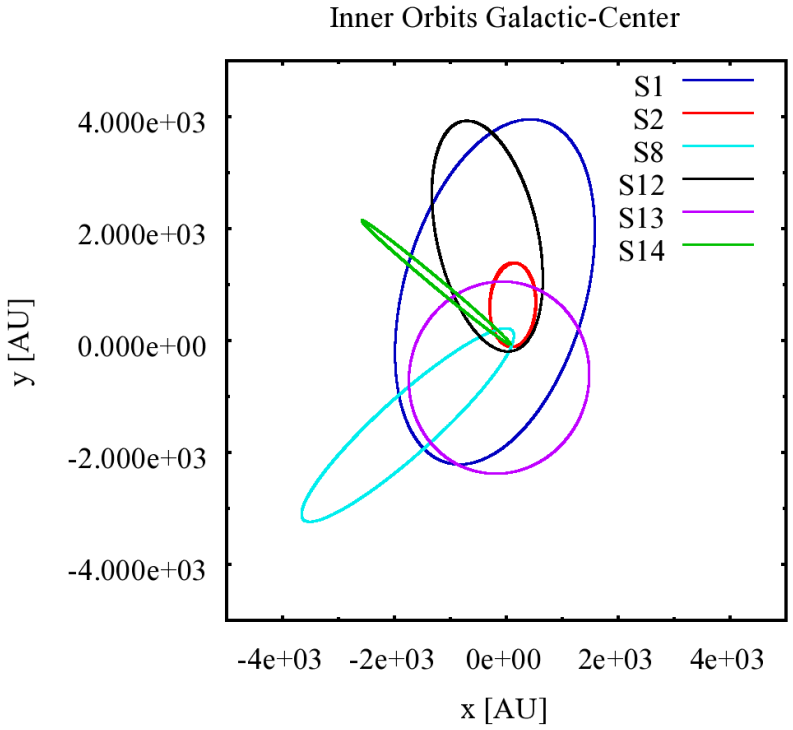

Figure 3.2: The Orbits of the inner 6 S-stars in x, y-projection

The x, y-projection, of isolated solutions, of the six 6 inner S-stars, using the initial values for the orbital parameters P, a, t_0, e, i, ω and Ω, from the publication of Eisenhauer et al. [20]. The positions of the S-stars: S1, S2, S8, S12, S13, S14; are plotted for t_0 to $t_0 + 100$ yr, with $t_0 = 2000$ yr.

As we see, the orbits of the isolated 'binaries' compare nicely to both the earlier generated orbits of the previous chapter and the literature. The earlier mentioned spikes in the solutions have no significant effect on the positions on the plane of the sky. We conclude that this HNBody artifact does not effect the overall character of the orbits of the S-stars.

3.3 Sgr. A* Star Cluster Evaluation

In this section we are going to use the HNBody code to evaluate a joint solution of the Sgr. A* star cluster. This 7-body configuration consists out of the SMBH plus the 6 previously mentioned S-stars. Similar to the previous section, we have evolved the system over the period $t = -10^3$ to 10^3 yr, with $t_0 = 2000$. In order to see if the orbits of the S-stars are no longer static, we have plotted the solutions of the positions over the periods $t = -10^3$ to -900, 0 to 100 and 900 to 10^3 (Fig. 3.3).

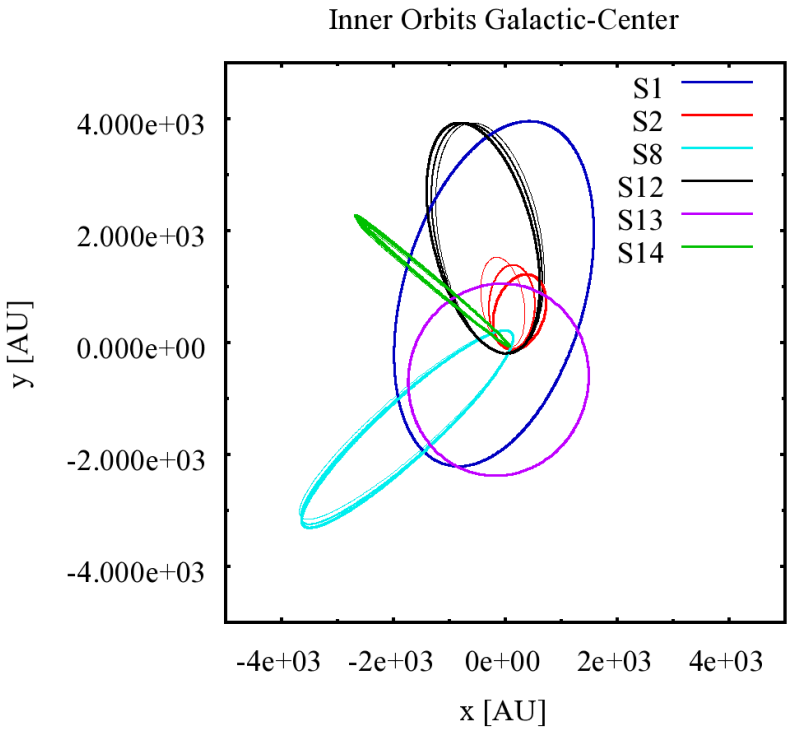

Figure 3.3: The Orbits of the inner 6 S-stars in x, y-projection

The x, y-projection of the positions of the six 6 inner S-stars, using the orbital parameters P, a, t_0, e, i, ω and Ω, of the original publication of Eisenhauer et al. [20]. The positions of the S-stars: S1, S2, S8, S12, S13, S14; are plotted for the period $t = -10^3$ to -900, 0 to 100 and 900 to 10^3, with respectively increasing line-width.

We see significant precession of three orbits [Fig. 3.3]. The orbits of S2, S8 and S12 have obviously rotated over this period of time. The precession of S2 is clearly the strongest and is estimated to be $\dot{\omega} \sim 0.015°$/yr on the plane of the sky.

Again we have plotted the *semi-major axis*, *eccentricity* and *inclination* over the same period -10^3 to $+10^3$ yrs. Resulting in the figures in Table 3.2.

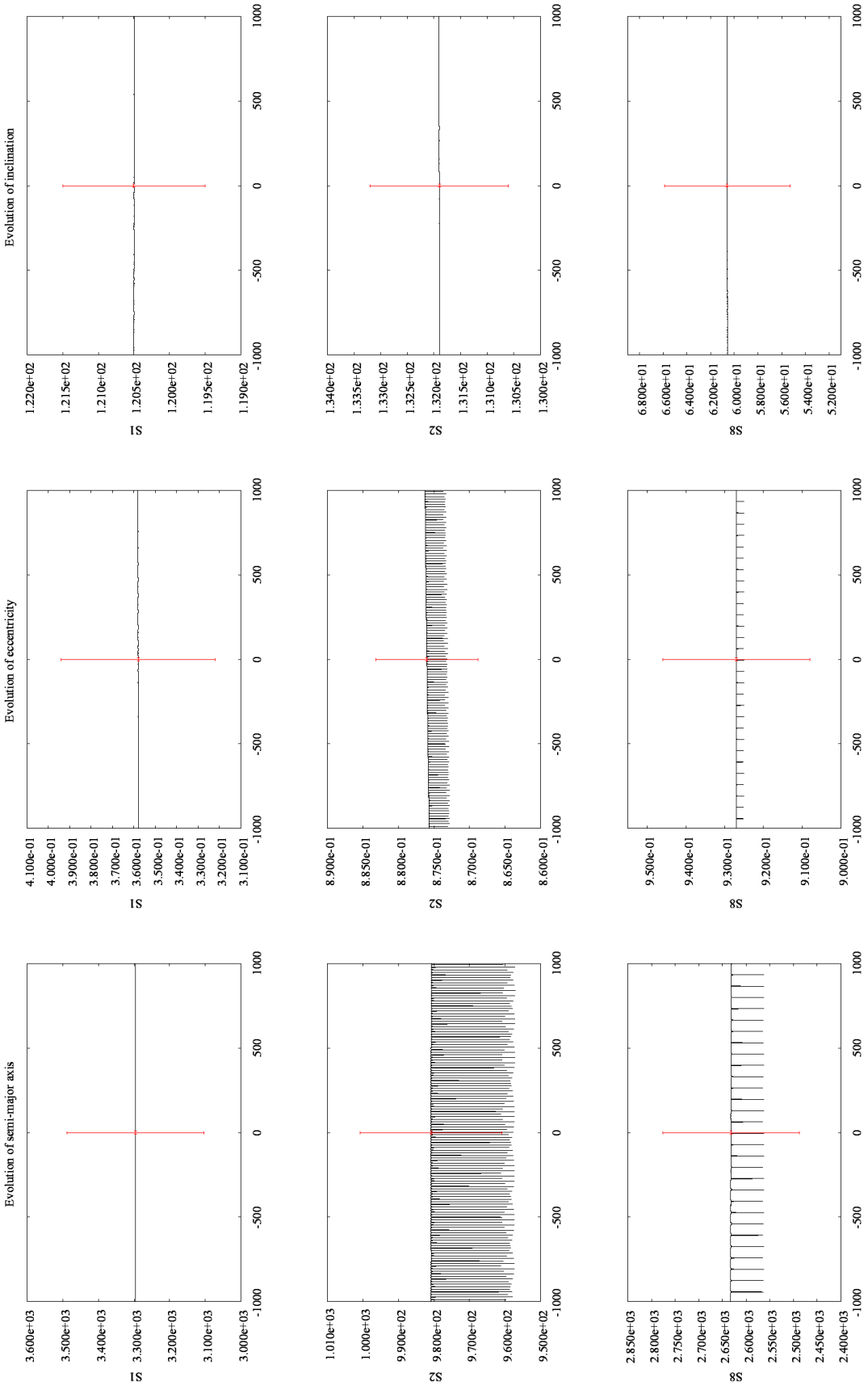
Evolution of inclination
Evolution of eccentricity
Evolution of semi-major axis
S1
S2
S8
1.220e+02
1.215e+02
1.210e+02
1.205e+02
1.200e+02
1.195e+02
1.190e+02
1.340e+02
1.335e+02
1.330e+02
1.325e+02
1.320e+02
1.315e+02
1.310e+02
1.305e+02
1.300e+02
6.800e+01
6.600e+01
6.400e+01
6.200e+01
6.000e+01
5.800e+01
5.600e+01
5.400e+01
5.200e+01
4.100e-01
4.000e-01
3.900e-01
3.800e-01
3.700e-01
3.600e-01
3.500e-01
3.400e-01
3.300e-01
3.200e-01
3.100e-01
8.900e-01
8.850e-01
8.800e-01
8.750e-01
8.700e-01
8.650e-01
8.600e-01
9.500e-01
9.400e-01
9.300e-01
9.200e-01
9.100e-01
9.000e-01
3.600e+03
3.500e+03
3.400e+03
3.300e+03
3.200e+03
3.100e+03
3.000e+03
1.010e+03
1.000e+03
9.900e+02
9.800e+02
9.700e+02
9.600e+02
9.500e+02
2.850e+03
2.800e+03
2.750e+03
2.700e+03
2.650e+03
2.600e+03
2.550e+03
2.500e+03
2.450e+03
2.400e+03
1000
500
0
-500
-1000

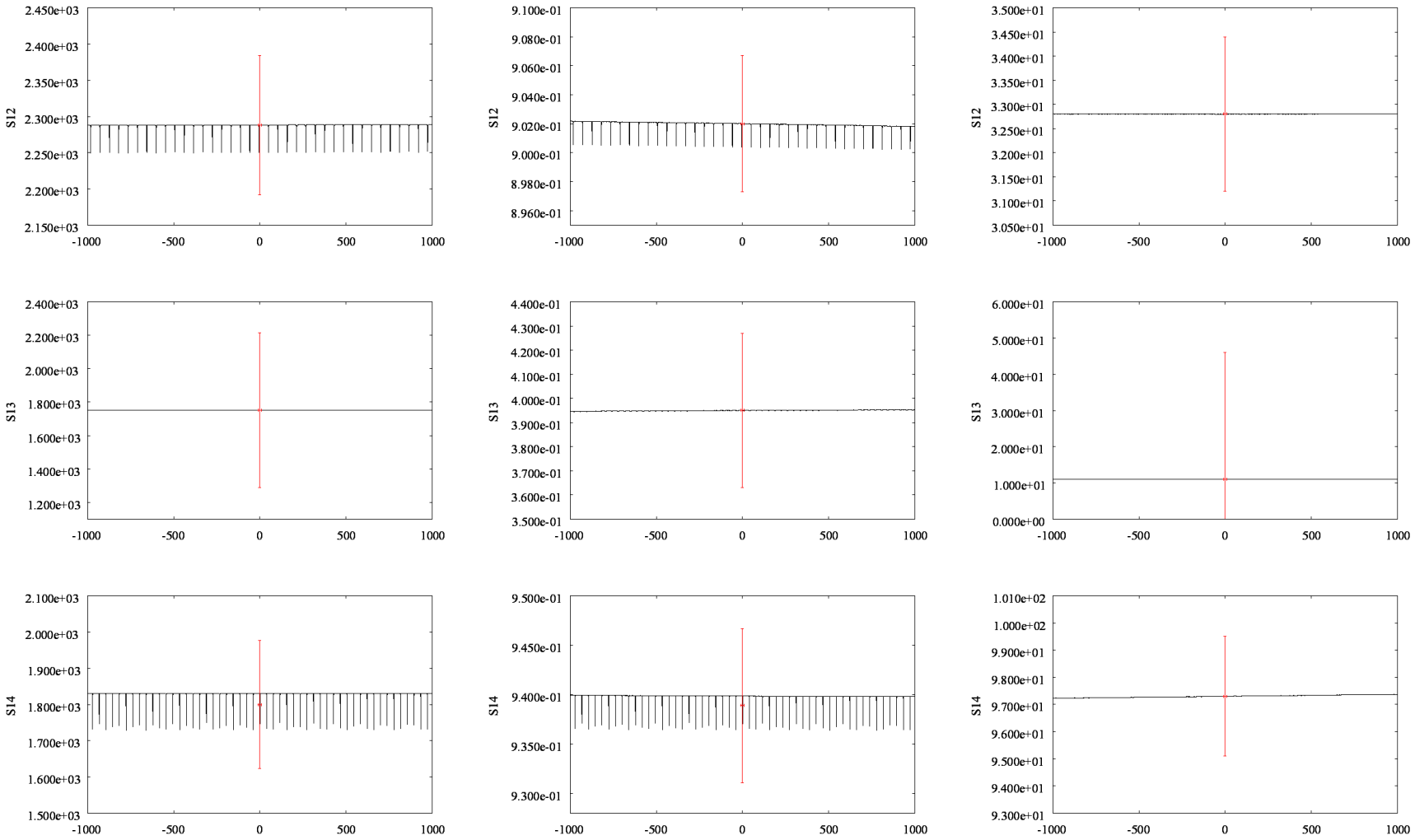

Table 3.2: The evolution of *semi-major axis*, *eccentricity* and *inclination* of the six inner 'S'-stars.

The evolution of *semi-major axis*, *eccentricity* and *inclination* of the six inner 'S'-stars, i.e. S1, S2, S8, S12, S13 & S14 under the influence of the SMBH. The solutions of this 7-body system are calculated over the period -10^3 to $+10^3$ yrs, with t_0 is the year 2000. The initial values for the orbital parameters at t_0, are taken from Eisenhauer et al. [20] and can be found in Table 2.2.1 on page 23.

It is clear that there is almost no evolution of these orbital parameters over this period of time. Only the $eccentricity$ of S2, S12 and S13 together with the $inclination$ of S14, show a minor variation compared to the uncertainty in the initial conditions. With S2 having the best constrained orbital parameters it shows a relative variation of a factor $\leq 3 \times 10^{-4}$. Besides the evolution of the orbital parameters, we have found that the system showed no significant resonances between any combination of S-stars. We therefore conclude that the system is stable.

As mentioned earlier, the error in the energy is a good indicator to check the stability and accuracy of the solution of the system. The evolvement of the energy, over the -10^3 to $+10^3$ yr period, is plotted in Fig. 3.4.

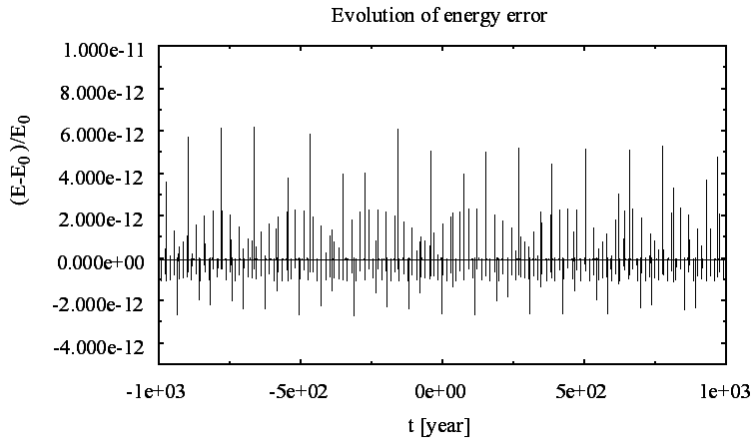

Figure 3.4: The error in system energy

The error in the energy of the joint solution of the 6 S-stars + SMBH for the period -10^3 to $+10^3$ yrs with t_0 the year 2000. The 7-body configuration is constructed by using the orbital parameters P, a, t_0, e, i, ω and Ω, from Eisenhauer et al. [20]. The mean value of the energy error is -9.10×10^{-14} with a standard deviation of $\pm 1\sigma = 2.32 \times 10^{-13}$.

We see the maximum deviation from zero, in the energy, is a factor of $\sim 6 \times 10^{-12}$. This is 10 times higher then the maximum energy error of the S2 + SMBH 'binary' configuration, as seen in the previous section. The mean value of the energy error is -9.10×10^{-14} with a standard deviation of $\pm 1\sigma = 2.32 \times 10^{-13}$. Comparing this to the isolated S2 - SMBH solution we see an increase in this relative error value. This is because all the energy errors in the individual S-star orbits contribute to the energy error of the joint solution. Nevertheless, the relative energy error of the joint solution is this still much smaller than the maximal relative uncertainty in the initial values for the orbital parameters. Because the the relative energy error is of an order $\sim 10^{-13}$ we assume the solution presented in Fig. 3.3 offers a good description of how the system would evolve as a result of the initial conditions from Eisenhauer et al. [20].

SMBH Positional and Velocity Variation for Time Evolution over -10^3 to $+10^3$ yrs

The variation in position of the SMBH, on the plane of the sky, during this period is small. The maximum reached distance from zero is $< 5 \times 10^{-2}$ AU (Fig. 3.5). The mean value of the distance from zero on the plane of the sky is $< x > = -1.98 \times 10^{-2}$ AU, with a standard deviation of $\pm 1\sigma = 8.3 \times 10^{-3}$ AU and $< y > = 1.24 \times 10^{-2}$ AU, with $\pm 1\sigma = 1.09 \times 10^{-2}$ AU. In order to detect this offset a resolution in the order of $\sim 10^{-8}$ arcsec would be necessary. This is so small we consider it to be far beyond the scope of the detectors (Weinberg, Milosavljević & Ghez [75]).

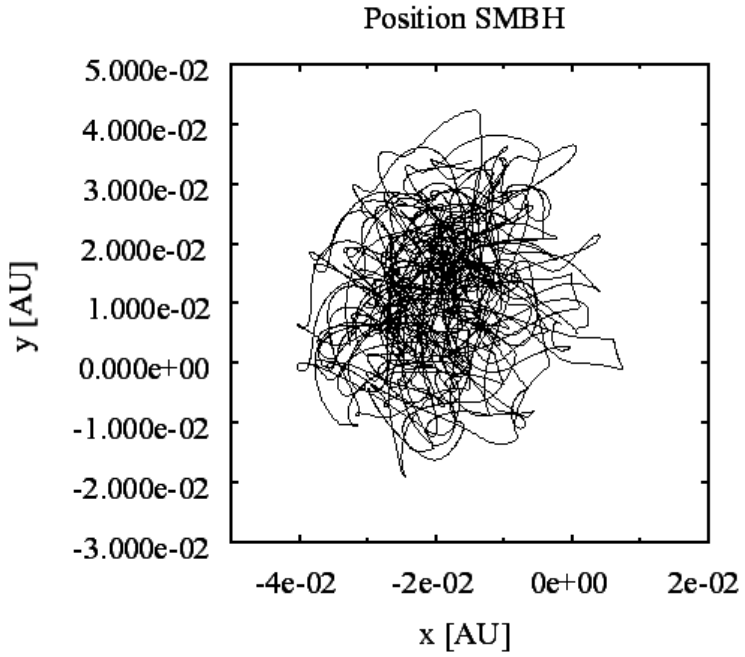

Figure 3.5: The variation of x, y-position of the SMBH

The x, y-projection of the position of the SMBH for -10^3 to $+10^3$ yrs. The SMBH is moving under the influence of the S-stars (i.e. S1, S2, S8, S12, S13 & S14). The 7-body configuration is initialized with the orbital parameters P, a, t_0, e, i, ω and Ω, from Eisenhauer et al. [20].

Taking a look at the velocity on the line of sight during this period, it shows a maximum velocity of 9×10^{-3} AU/yr ($t \simeq -700$ yrs and 500 yrs) , which is $\sim 4.3 \times 10^{-2}$ km s^{-1} (Fig. 3.6 on the next page). The mean velocities and standard deviations, in all three directions are respectively: $v_x = 9.54 \times 10^{-5}$ AU yr^{-1}, with $\pm\sigma = 1.58 \times 10^{-3}$ AU yr^{-1}, $v_y = -1.17 \times 10^{-4}$ AU yr^{-1} with $\pm\sigma = 1.90 \times 10^{-3}$ AU yr^{-1} and $v_z = -6.37 \times 10^{-6}$ AU yr^{-1}, with $\pm\sigma = 1.28 \times 10^{-3}$ AU yr^{-1}.

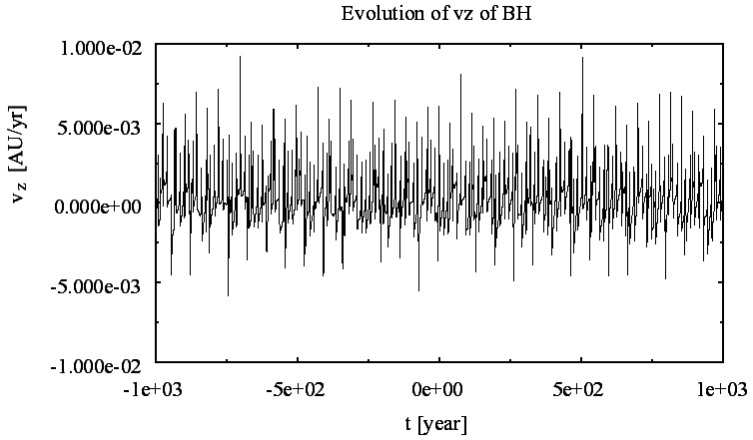

Figure 3.6: The velocity of the SMBH on the line of sight

The velocity of the SMBH on the line of sight due to the influence of the S-stars (i.e. S1, S2, S8, S12, S13 & S14). $v_{z,SMBH}$ is plotted over the period -10^3 to $+10^3$ yrs. Initial values of the orbital parameters, P, a, t_0, e, i, ω and Ω, are taken from Eisenhauer et al. [20]. Note that $1\,AU/yr \simeq 4.7\,kms^{-1}$.

The motion in the galactic plane, consisting out of our v_x and v_y values, is small compared to value of the motion in the literature of 3.8 ± 1.5AU yr^1. Though deviating less, the motion perpendicular to the galactic plane (v_y) of $8.410^{-2} \pm 0.18$AU yr^1 is also small (Reid et al [62], Reid & Brunthaler [64]). The velocities induced by the orbital movement of the S-stars contribute only a fraction to the observed values of motion. Future research is necessary to understand why this deviation occurs. Earlier estimated values of the velocity of Sgr. A* by Ghez et al. [27]) resulted in values up to 12.7 ± 4.2 AU yr^{-1}. More recent work suggested that this could be accounted for by a locally heated dust feature (Ghez et al. [28]). Our solution to the velocity of the SMBH seem to favor the latter.

3.3.1 Long Term Stability of the System

In this part, we are going to take a look at the long-term, -10^5 to $+10^5$ yr, stability and evolution of the 7-body system. The evolution of the energy-error over this long period, see Fig. 3.7 on the next page, has a maximum relative error of a factor 9.5×10^{-10}. Although this is a slight increase compared to the period of -10^3 to $+10^3$ yr, it is again much smaller then the accuracy in the initial values for the orbital parameters. With an average value of the relative error -9.37×10^{-14} and a standard deviation 1σ of 2.38×10^{-13} and speaking in terms of relative energy

errors it's almost identical to the -10^3 to $+10^3$ yr period. Therefore we conclude that the HNBody code will keep its accurate behavior over this long period.

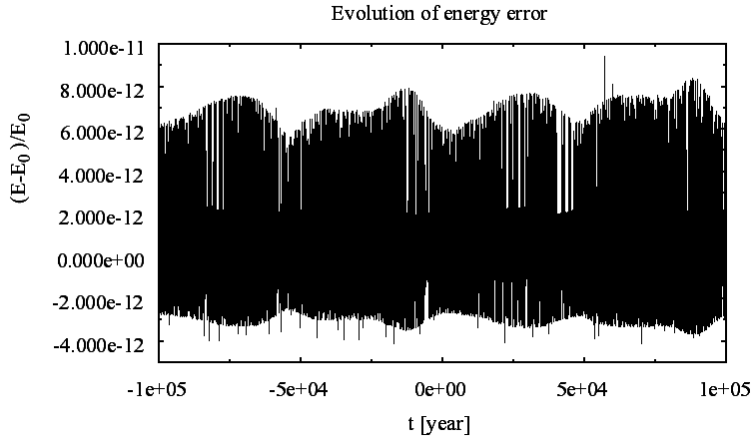

Figure 3.7: The error in system energy

The error in the energy of the 6 S-stars + SMBH configuration, for -10^5 to $+10^5$ yrs. The offset from center of the SMBH is a result of the S-stars positioning. The joint 7-body configuration is based on the orbital parameters P, a, t_0, e, i, ω and Ω, from Eisenhauer et al. [20].

Again we take a look at the evolution of the $semi\text{-}major\ axis$, $eccentricity$ and $inclination$ of the six inner S-stars. When interpreting the solutions, we should keep in mind that we are working with a simplified model of Sgr. A* cluster. The solutions are purely based on the dynamics of the S-stars. For solutions closer to reality, we should for instance consider mass loss due to stellar evolution. As shown by Cuadra et al. [13], the mass loss rate of the S-stars could be significant over this time period. In a more sophisticated model the stellar evolution would lead to a change in momentum and fill the ISM with the stellar winds of the S-stars. Besides this is not yet feasible due to computational limits, it is beyond the scope of this work. The solutions of the three earlier mentioned orbital parameters are presented in the Table of figures 3.3 on the next two pages.

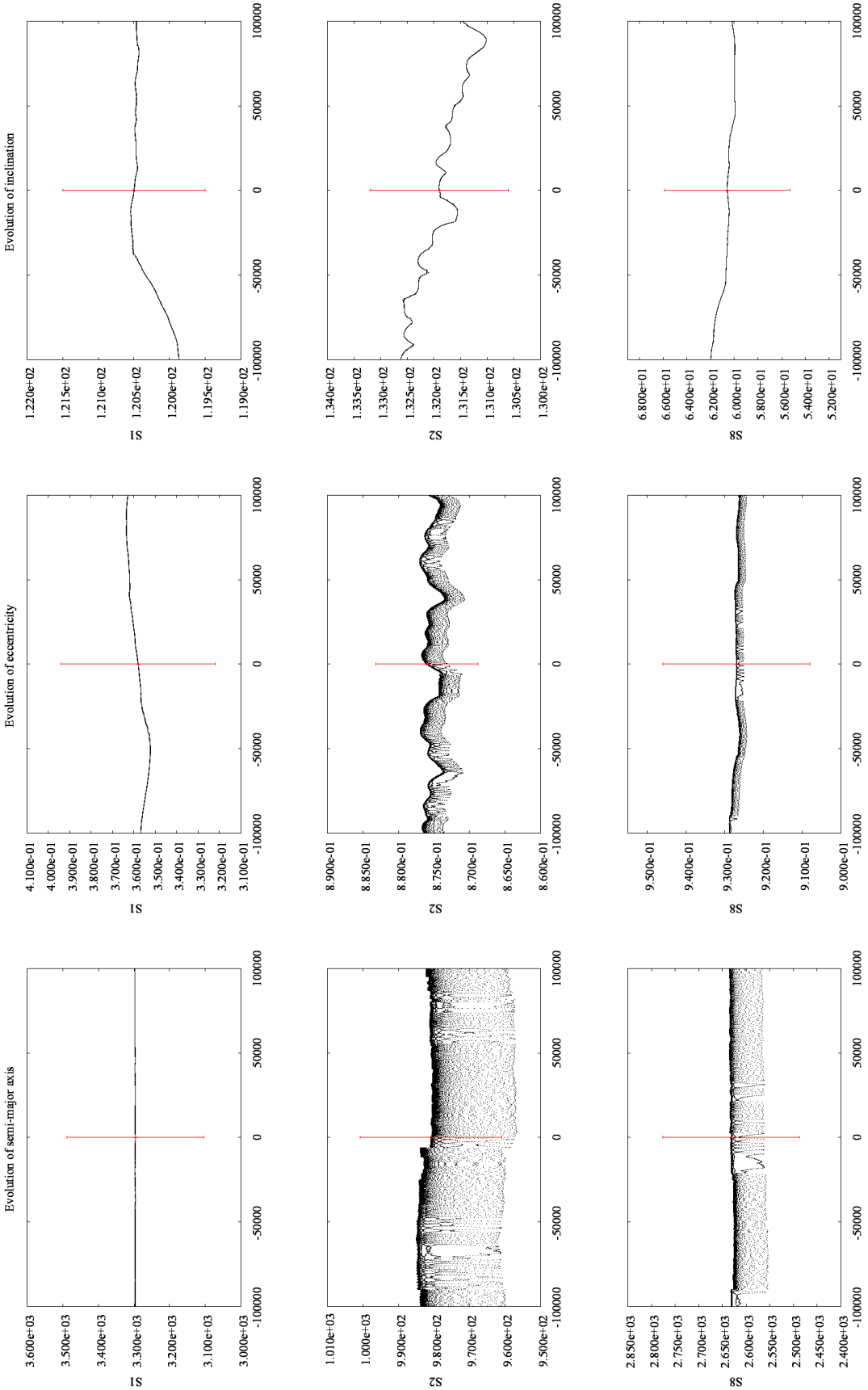
Evolution of inclination
Evolution of eccentricity
Evolution of semi-major axis
S1
S2
S8
1.220e+02
1.215e+02
1.210e+02
1.205e+02
1.200e+02
1.195e+02
1.190e+02
1.340e+02
1.335e+02
1.330e+02
1.325e+02
1.320e+02
1.315e+02
1.310e+02
1.305e+02
1.300e+02
6.800e+01
6.600e+01
6.400e+01
6.200e+01
6.000e+01
5.800e+01
5.600e+01
5.400e+01
5.200e+01
4.100e-01
4.000e-01
3.900e-01
3.800e-01
3.700e-01
3.600e-01
3.500e-01
3.400e-01
3.300e-01
3.200e-01
3.100e-01
8.900e-01
8.850e-01
8.800e-01
8.750e-01
8.700e-01
8.650e-01
8.600e-01
9.500e-01
9.400e-01
9.300e-01
9.200e-01
9.100e-01
9.000e-01
3.600e+03
3.500e+03
3.400e+03
3.300e+03
3.200e+03
3.100e+03
3.000e+03
1.010e+03
1.000e+03
9.900e+02
9.800e+02
9.700e+02
9.600e+02
9.500e+02
2.850e+03
2.800e+03
2.750e+03
2.700e+03
2.650e+03
2.600e+03
2.550e+03
2.500e+03
2.450e+03
2.400e+03
100000
50000
0
-50000
-100000

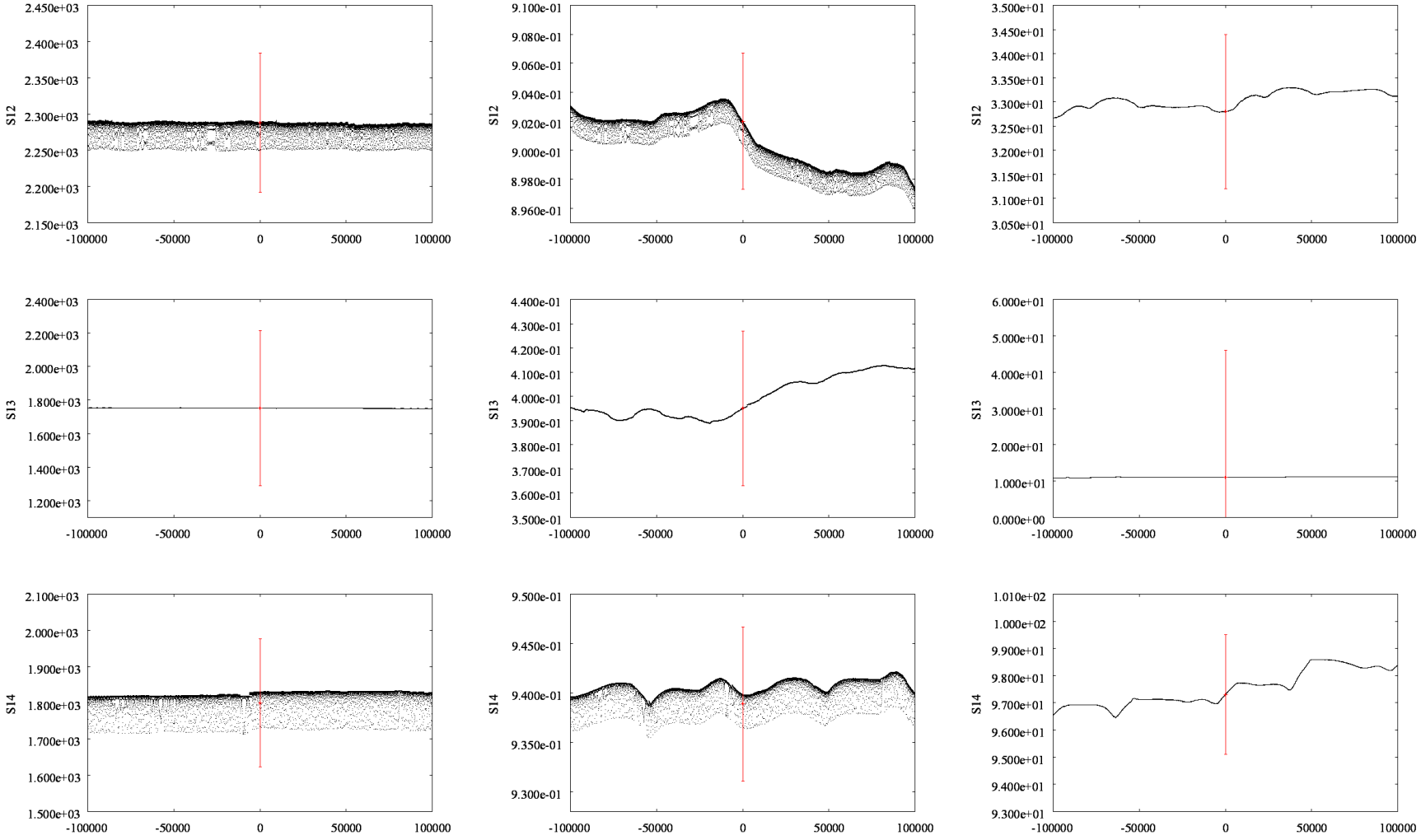

Table 3.3: The evolution of *semi-major axis*, *eccentricity* and *inclination* of the six inner 'S'-stars.

The evolution of *semi-major axis*, *eccentricity* and *inclination* of the six inner 'S'-stars. The period ranges from -10^5 to $+10^5$ yr, with $t_0 = 2000$. The initial conditions for this system, are from Eisenhauer et al. [20]. The *eccentricity* of S12 shows the strongest variation, compared to the accuracy of the initial condition. However, even over a period of 10^5 yr, this variation in *eccentricity* will not exceed the accuracy in its initial value. The occurring 'bandwidth' in the related figures are due to an artifact of HNBody.

As can be seen in the figures, the $eccentricity$ of S12 shows the strongest variation compared to the accuracy of the initial condition. However, even over a period of 10^5 yr, this variation in $eccentricity$ will not exceed the accuracy this orbital parameter. Note that the system seems to favor the increase the eccentricity of the two least eccentric orbits of S1 and S13.

Equal to the -10^3 to 10^3 epoch, we calculated the the mean line of sight velocity $< v_z >= 5.68 \times 10^{-8}$ AU yr^{-1}, with $\pm\sigma = 1.40 \times 10^{-3}$ AU yr^{-1}. The results are plotted in Fig. 3.8. The values for the velocities in this period compared to the values for the -10^3 to 10^3 period, show a mean value which is smaller and a standard deviation of the same order. This is also true for the mean velocities on the plane of the sky: $< v_x >= -4.75 \times 10^{-8}$ AU yr^{-1}, with $\pm\sigma = 1.57 \times 10^{-3}$ AU yr^{-1} and $< v_y >= 7.18 \times 10^{-7}$ AU yr^{-1}, with $\pm\sigma = 1.63 \times 10^{-3}$ AU yr^{-1}.

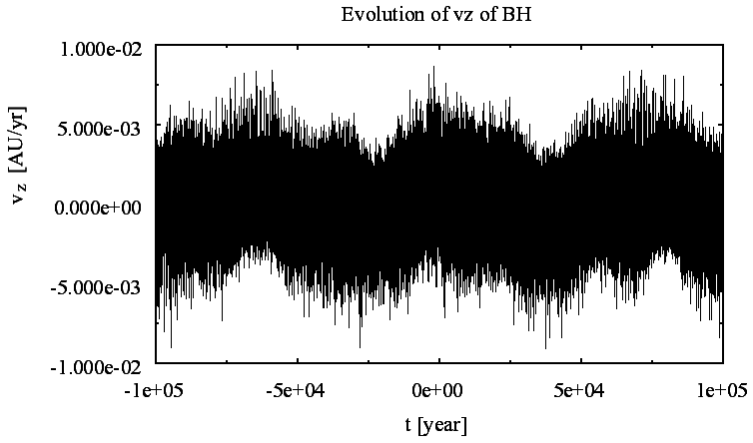

Figure 3.8: The velocity of the SMBH on the line of sight

The velocity of the SMBH on the line of sight due to the influence of the S-stars (i.e. S1, S2, S8, S12, S13 & S14). $v_{z,SMBH}$ is plotted over the period -10^5 to $+10^5$ yrs. The joint solution of the 7-body configuration, is based on the orbital parameters P, a, t_0, e, i, ω and Ω, from Eisenhauer et al. [20]. Note. $1\,AU/yr \simeq 4.7\,kms^{-1}$

Finally, the displacement of the SMBH on the plane of the sky (see Fig. 3.9), over this long period is difficult to compare with the the previous period (2×10^3 yrs, Fig. 3.5). The long-term displacement results in to much information in the figure. To be able to compare both periods, we present the mean values and standard deviations of the position of the SMBH over this epoch : $< x >= 6.54 \times 10^{-3}$ AU/yr, with $\pm\sigma = 1.13 \times 10^{-2}$ AU, $< y >= 1.82 \times 10^{-3}$ AU, with $\pm\sigma = 1.22 \times 10^{-2}$ AU and $< z >= 5.0 \times 10^{-3}$ AU, with $\pm\sigma = 1.26 \times 10^{-2}$ AU. There is a slight increase in the value for the mean distance. However, the maximum

offset is of the same order as in the '$-10^3, 10^3$' period.

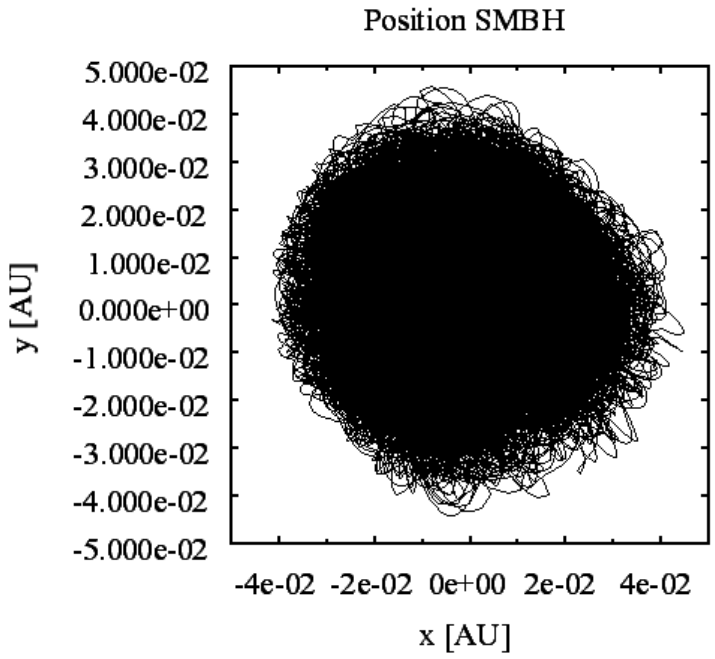

Figure 3.9: The variation of x, y-position of the SMBH

The x, y-projection of the position of the SMBH for $10^{-5} \leq t_0 \leq 10^5$ yrs, with $t_0 = 2000\, yrs$. The SMBH is moving under the influence of the S-stars. The initial 7-body configuration is constructed with the use of the orbital parameters P, a, t_0, e, i, ω and Ω, from Eisenhauer et al. [20].

Chapter 4

Dark Matter at the Galactic Center

4.1 Introduction

As mentioned in Chapter 1, the Milky Way harbors a great amount of dark matter. The way this dark matter is distributed at the Galactic center (GC) has been a point of interest for years. A study in this field of interest by Miralda-Escudé & Gould [48], had an outcome that the central parsec could harbor up to 24,000 stellar mass black holes. A more recent study, on the mass distribution in central arcsec, showed that most of its mass is dark and is contained within the supermassive black hole (SMBH) (Schödel et al. [67]). A consequence of their method was that besides the SMBH, a 1σ limited value up to 5×10^5 $M_\odot$ could be present at inner 0.1 pc of the GC. This could have serious consequences for the dynamical properties of the S-stars.

With in mind this possibility of more mass at the GC, we took another look at one particular solution to the 'Paradox of Youth': the inspiraling cluster scenario (ICS) proposed by Portegies Zwart, McMillan & Gerhard [57]. This scenario accounts for the presence of the young S-stars at the GC by the inspiraling of a second black hole which dragged the S-stars to their observed location. As mentioned at the end of Chapter 1, the presence of young stars in the vicinity of the SMBH is unaccounted for by present models of starformation. Extending work on the ICS by Hansen & Milosavljević [34] resulted in an example of this scenario to account for the presence of S2. They showed that it would require a black hole of 4×10^3 $M_\odot$ to transport S2 within a distance of 0.01 pc from SMBH. This is well within the earlier stated 1σ limit on the mass at the GC derived by Schödel et al. [67]. The mass of this 'necessary' black hole is within the typical mass range of intermediate mass black holes (IMBHs), which ranges from $\sim 10^2$ to $\sim 10^4$. We will therefore refer to these more massive objects, in the ICS, as IMBHs.

Besides that inspiraling IMBHs could explain the presence of S-stars, it could

also give a new explanation for the existence of the SMBH itself. It is thought that SMBHs are formed through the mergers of IMBHs (M. Atakan Gürkan & F. A. Rasio [33]). This makes the ICS an even more complete model for the formation of the Sgr. A* star cluster.

In this chapter we are going to extend our model of the Sgr. A* cluster with 'dark' objects and evaluate their influence on the SMBH and S-stars with the HNBody code. We are especially interested in the possibility of a hidden IMBH in the system. If the SMBH and S-stars prove to be indifferent to the extra dark objects, the ICS upholds. On the other hand, if our model of the system shows strong deviations under the influence of these dark objects we can exclude the inspiraling cluster scenario as a solution to the "Paradox of Youth".

4.1.1 HNBody Evaluations of Extra Mass in the Sgr. A* Cluster

Equal to chapter 3, we are going to look at the three orbital parameters *semi-major axis*, *eccentricity* and *inclination*. The extra mass should influence the characteristics of the orbits. The induced variation in the solutions of these parameters, due to the added mass in the system, can be compared with the solutions from Chapter 3 and the observational values from Eisenhauer et al. [20]. In this study we look specifically at the time period $-10 \leq t_0 \leq 10$ yrs, with t_0 being the year 2000. This period overlaps the observations so far and predicts evolution just before the observations and especially in the near future.

Although any configuration of extra mass should manifest it's presence on the orbits of the S-stars we do not know the sensitivity of the Sgr. A* cluster to this extra mass. Therefore we start with the evaluation of the less massive stellar mass BHs. We place[1] 10 black holes with a typical mass of 7 $M_\odot$ (Miralda-Escudé & Gould [48]). The orbital parameters, of the stellar mass black holes, are restricted to a sphere around the SMBH with a radius of 8×10^3 AU, which contains the full orbits of the S-stars.

Based on the isotropic behavior of the S-stars we use, except for the eccentricity, random initial parameters for these stellar mass BHs (Ghez et al. [29]). For the eccentricity we take an upper limit of 0.9 to avoid encounters with the SMBH. As mentioned in the previous chapter the handling of encounters is a known weakness of the symplectic integrator.

As a measure of significance, we take the standard deviation of the induced variations in the orbital parameters (σ_{S-star}), divided by the uncertainties in their initial values (σ_{obs}). If this value, $\sigma_{S-star}/\sigma_{obs} > 2.5$, we consider the influence of the dark objects to be detectable.

[1] The implementation of an extra objects in the system is done by adding a line at the initial conditions in the input file of HNBody (page 37) with the right orbital parameters and mass.

The result, of the extra stellar mass BHs, on the orbital parameters of the S-stars is insignificant ($\sigma_{S-star}/\sigma_{obs} << 1$). The extra mass of the BHs, compared to the dominant 4.06×10^6 $M_\odot$ of the SMBH, is too small to influence the orbits of the S-stars.

When we use the same setup as above but with high eccentricities ($0.9 < e < 1.0$), we see the effect of encounters. Strange anomalies like negative values for the semi-major axis show up in the output. There the HNBody code is not equipped with the handling of these encounters, this is beyond the scope of this study and is mentioned for future research.

4.2 The Inspiraling Cluster Scenario

As mentioned earlier, we are especially interested in the inspiraling clusters scenario as an origin of the S-stars. The related Intermediate Mass Black Hole (IMBH) which guided the S-stars to the GC could still be present in the vicinity of the SMBH. Therefore we add an IMBH to the 7-body system from the previous chapter and calculate the effect this object has on the now 8-body system. Again we take specific interest in the three orbital parameters: semi-major axis, eccentricity and inclination of the six S-stars and use the same measure for the significance as for the evaluation of the added stellar mass BHs.

In the previous section we found that the influence of extra mass in the form of stellar mass black holes is insignificant compared to the observational uncertainties. A much more massive object like an IMBH, will have more effect and reveal it's presence by perturbing the orbital parameters of the S-stars. As an example we show the anomalies in the semi-major axis of S14, as a result from the presence of an IMBH orbiting the SMBH at a distance of 60 AU (Fig. 4.1).

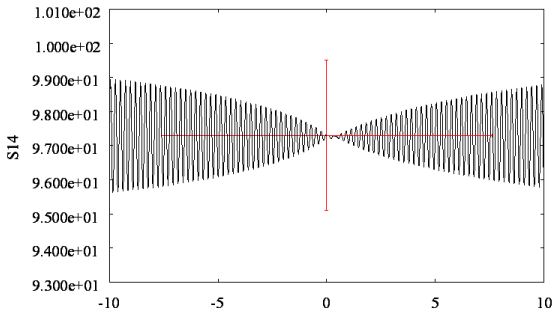

Figure 4.1: Induced periodic anomalies in the semi-major axis of S14

The periodic movement of the semi-major axis of S14 is caused by the presence of an orbiting IMBH. In this example the 'periodic induced anomaly' is induced by adding an IMBH of 1000 $M_\odot$ at a distance of 60 AU from the SMBH

4.2.1 Limits on the Phase-space Coordinates of the IMBH

In choosing the orbital parameters for the IMBH, there are somethings to reckon with. Again we want to elude encounters and therefore set the eccentricity to zero and choose specific values for the semi-major axis. We have evaluated the IMBH with a semi-major axis of 40, 60, 80 and 100 AU, which is small enough not to encounter S2 in its orbit and large enough not to merge with the SMBH[2]. Note that as a result the orbital period of the IMBH will be much smaller then that of S2, which has the smallest period of the S-stars.

A massive orbiting IMBH will effect the position of the SMBH. Due to a shift in barycenter the SMBH will show a reflex "motion". The velocity of the SMBH perpendicular to the galactic plane is limited to $-8.4 \times 10^{-2} \pm 0.18$ AUyr^{-1} (Reid & Brunthaler [64]). This value limits the initial conditions for the combination of the inclination, distance and mass of the IMBH. A highly inclined orbiting massive object would cause a reflex motion of the SMBH perpendicular to the galactic plane. We therefore have investigated the influence of an IMBH with a typical mass of 10^2 to 10^5, with a semi-major axis of 40, 60, 80, and 100 AU. Because the velocity in the galactic plane has a much higher value of 3.8 ± 1.5 AUyr^{-1} we exclude inclinations $< \pm 5°$. The results are presented in Fig. 4.2 on the next page.

As can be seen the inclination is restricted by the mass and semi-major axis of the IMBH. Therefore the inclination also restricts the maximal mass of the IMBH. Because we are especially interested in the maximal value for the mass of the IMBH, we take the inclination to be zero. As a result of the zero eccentricity and inclination, the other orbital parameters, line of nodes Ω and argument of periastron ω, will not influence the character of the orbit.

[2]Future work could be done on the timescale of mergers and the effect of gravitational wave radiation.

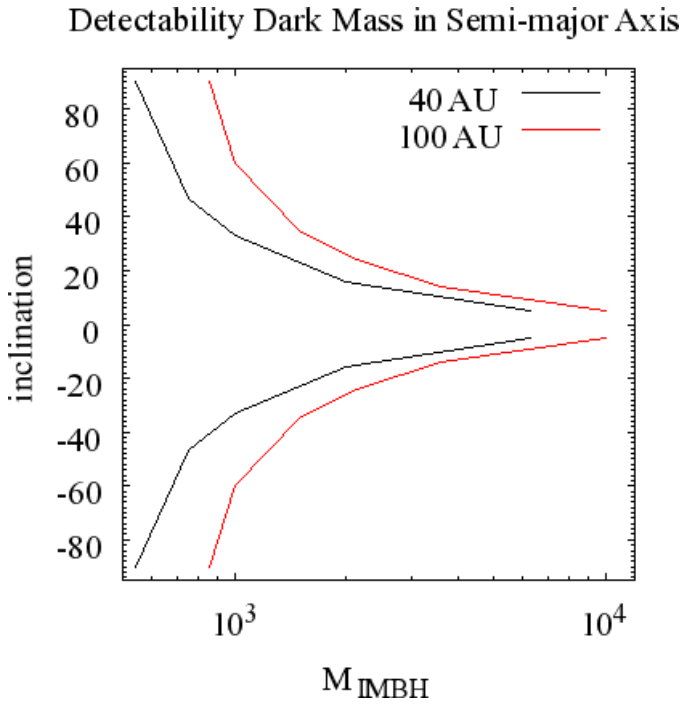

Figure 4.2: Limits on inclination of the 'extra' IMBH

Limits on the inclination of an IMBH compared to its mass. The line represents $\sigma_{S-star}/\sigma_{obs} = 1$ for an inclination between $-5^\circ \leq i \leq -90^\circ$ and $5^\circ \leq i \leq 90^\circ$, of the IMBH. Red line indicates limit for an IMBH located at 100 AU and black line indicates the limit at 40 AU. The limit on the velocity is $-8.4 \times 10^{-2} \pm 0.18$ AUyr^{-1} (Reid & Brunthaler [64]). The mass of the IMBH is in units of $M_\odot$.

4.2.2 Perturbations in the Solutions due to an IMBH at the Galactic Center

We now have set the limits on the orbital parameters of the IMBH. As mentioned earlier we are going to evaluate the three orbital parameters of the S-stars mentioned at the beginning of this section. For the measure of significance we take again ($\sigma_{S-star}/\sigma_{obs}$. We investigated the "detectability" of the IMBH for the masses; 10^2, 10^3, 10^4 and 10^5. Together with a semi-major axis of; 40, 60, 80 and 100 AU, and the an eccentricity and inclination of zero. We present the results on the next three pages. The added the line of 1σ for reference.

Detectability in the Semi-major Axis

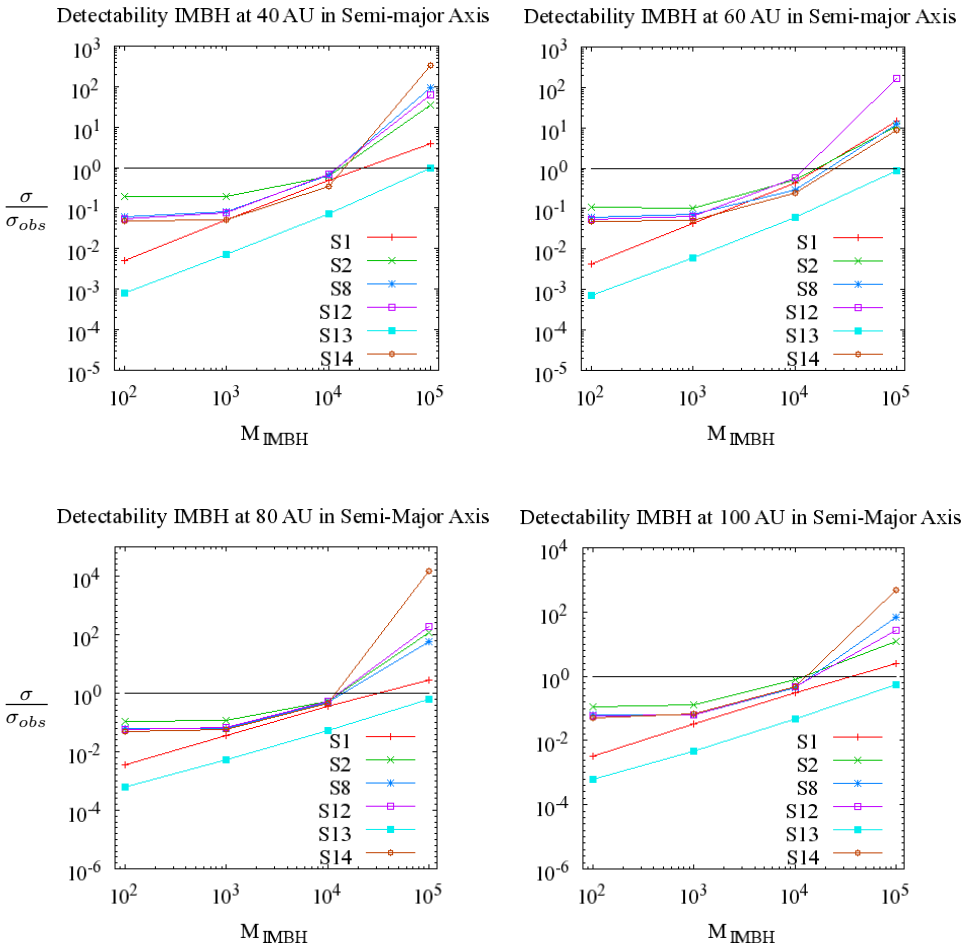

Table 4.1: Detectability of an IMBH in the Semi-major Axis of the S-stars

Detectability of added dark mass in the semi-major axis of the S-stars. Induced deviations due to the placing of an IMBH at 60 AU from the SMBH.

Detectability in the Eccentricity

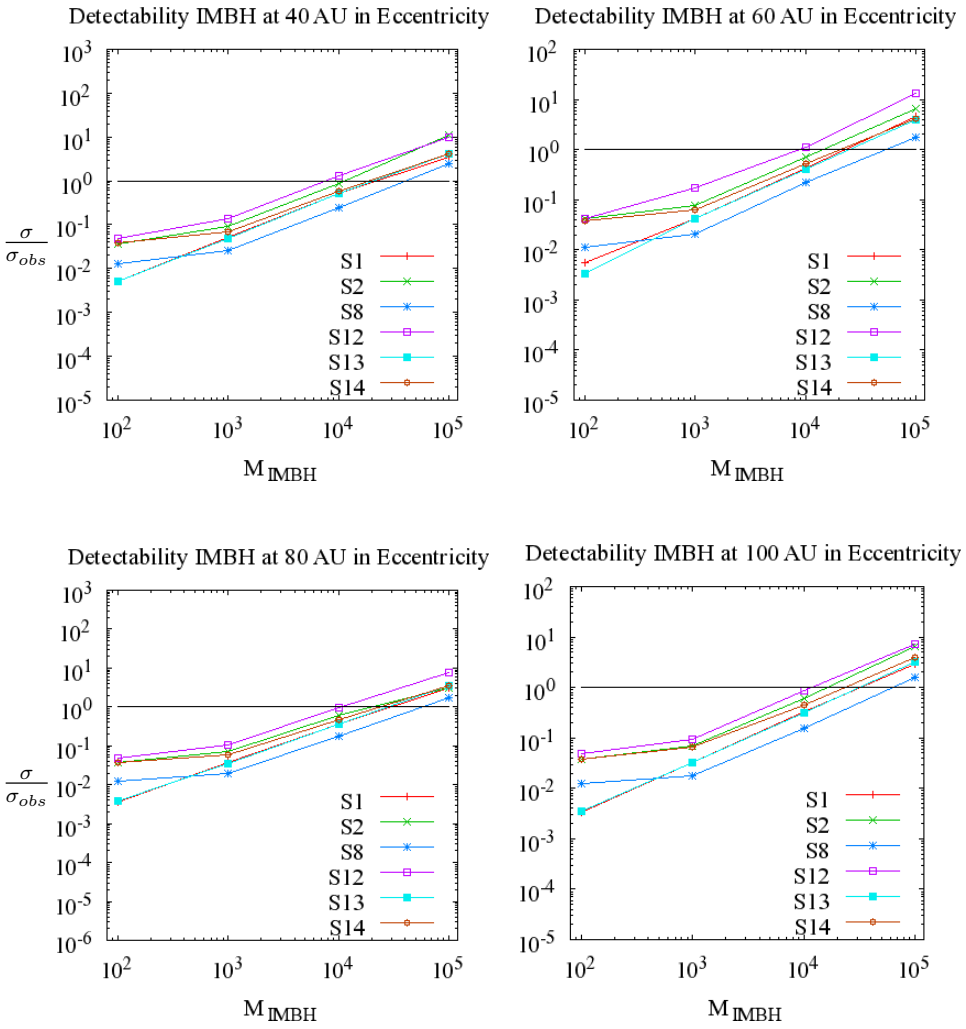

Table 4.2: Detectability of an IMBH in the Semi-major Axis of the S-stars

Detectability of added dark mass in the semi-major axis of the S-stars. Induced deviations due to the placing of an IMBH at 60 AU from the SMBH.

Detectability in the Inclination

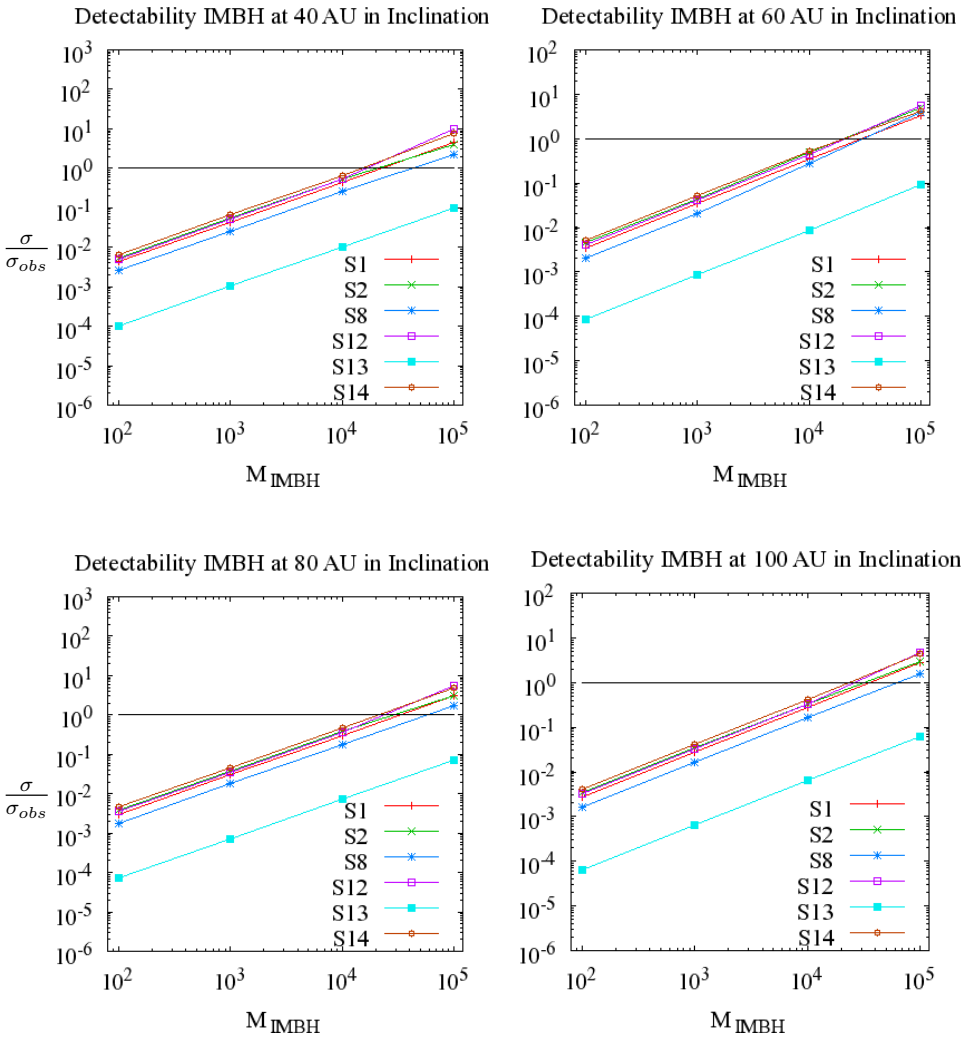

Table 4.3: Detectability of an IMBH in the Semi-major Axis of the S-stars

Detectability of added dark mass in the semi-major axis of the S-stars. Induced deviations due to the placing of an IMBH at 60 AU from the SMBH.

As can be seen in all the parameters a IMBH of $\sim 10^4$ $M_\odot$ reaches the limit of detection. We see that the eccentricity of the S-stars is the most sensitive to the added mass. The earlier stated configuration of the IMBH with a mass of $\sim 10^4$ causes a change in the eccentricity of S12 which would be detectable. This compares well with the findings of Lu et al. [43]. They found restrictions on the inspiraling cluster scenario for a distance < 0.08 pc ($\sim$16000); a cluster could not have $> 10^4$ $M_\odot$ due to reflex motion of Sgr. A^*.

So we have found that besides the so called reflex motion of the SMBH, the orbital parameters of the S-stars are equally sensitive to the presence of an IMBH. Furthermore the presence of stellar mass black holes elude our detection unless they encounter one of the S-stars. These encounter would directly effect the orbit of the S-star. Study on the expected rate of these encounter would be desirable.

So, the presence of stellar mass black holes can only be seen in two cases. When the merge with the SMBH or when the encounter one of the S-stars. This is due to their relative low mass compared to the SMBH. On the other hand, we have found that besides the motion of the SMBH, the orbital parameters are equally sensitive to the presence of an IMBH. Of the S-stars the overall most sensitive one is S12.

Chapter 5

Conclusion

5.1 Results

As we have seen the Galactic Center contains a variety of extraordinary objects. From the most dense stellar clusters known in the Milky Way to the extreme conditions of the inner arcsecond. In this 'inner' part of the Galactic Center the closest candidate for a supermassive black hole is found. With an mass of $\sim 4 \times 10^6$ $M_\odot$ it is orbited by young stars with velocities up to 9,000 kms^{-1}. This strange combination of young, so called, S-stars in the vicinity of the supermassive black hole has raised questions about their origin. The standard starformation models are not sufficient to explain this so called "Paradox of Youth".

Using the Kepler equations we derived a semi-analytical solution for the positions and velocities of six S-stars orbiting the supermassive black hole (SMBH). We implemented this method into a C++ code to present projections of the orbits which are in excellent agreement to the literature. As this method provides a static solution, based on the orbital parameters, we evaluated the system with a more advanced one. Based on the conservation of the Hamiltonian the HNBody code provides, by means of symplectic integration, an accurate time-dependent joint solution for the evolution of this stellar cluster.

As we analyzed the system over a period of $-10^5 \leq t_0 \leq +10^5$ yrs, it became clear that system is very stable under its initial conditions. In this long-term integration, the HNBody code provides accurate solutions of the orbital parameters. Over this period, the values of the orbital parameters stayed within the $\pm 1\sigma$ uncertainties in their initial values.

The properties of the Sgr. A^* cluster enables us to use two independent methods to find an upper limit to the mass of dark objects hiding in the vicinity of the SMBH. The first method makes use of the limited velocity of the SMBH perpendicular to the galactic plane. Because orbiting massive objects cause a reflex motion of the SMBH the inclination of the IMBH is limited to it's mass and distance. Using the value of -0.4 ± 0.9 kms^{-1} from Reid & Brunthaler [64] we found that a circular orbiting IMBH at 100 AU with a mass $> 5 \times 10^3$ $M_\odot$ and an inclina-

tion $> \pm 5^{\circ}$, induces a motion of the SMBH which exceeds the observational value.

The second method is makes use of the uncertainties in the orbital parameters. Massive objects induce anomalies in the orbital parameters. When the standard deviation of these anomalies significantly exceed the uncertainties in the observational values, they are detectable. With this method we found that stellar mass black holes show a currently observationally undetectable influence on the Sgr. A* cluster ($\sigma_{S-star}/\sigma_{obs} << 1$). On the other hand, the more massive intermediate mass black holes (IMBHs) show their presence depending on the values of the phase-space coordinates. Resulting in that the inspiraling cluster scenario as a solution to the "Paradox of Youth" is possible under certain conditions.

Besides this we have found a limit on the mass for hiding an IMBH within a 100 AU distance from the SMBH. This is derived from adding an IMBH with masses from 10^2 to 10^5 $M_{\odot}$ at the distances of 40, 60, 80 and 100 AU from the SMBH. The presence of an IMBH caused anomalies in the solutions provided by the HNBody code. When the value of these induced anomalies exceed the uncertainty in one of the orbital parameters we considered them to be detectable $\sigma_{S-star}/\sigma_{obs} > 1$. In other words, over the measured period they should have been detected. In this method it shows that the inclination of the orbital parameters is least effected by the adding of an IMBH. The most effect is generated in either one of the other evaluated orbital parameters. The method results for all configurations in a limit of $\sim 10^4$ $M_{\odot}$ as being detectable.

5.2 Discussion

As seemed that the anomalies are induced by the rapid orbiting of the IMBH the method itself seems limited to configuration where $P_{IMBH} << P_{S-star}$. Though the agrees excellent with the literature (Lu et al. [43]), we cannot account for the influence of an artifact of the HNBody code. Although the relative errors in the solution of the HNBody code are of an order 10^{-11}, the in Chapter 3 described peaks could have their influence on the solutions for the orbital parameters. Study on these peaks showed that decreasing the time-steps to 1×10^{-7} did not remove these artifacts. The only way to remove the peaks from the output was to decrease the mass of the dominant object or by lowering the eccentricities of the S-stars. Thus changing the properties of the system. Long-term integration of system shows the stability of the energy. We conclude that the overall effect of the artifacts can be neglected compared to the induced anomalies, our method provides an alternative way to restrain the dark mass at the Galactic Center.

This new alternative method we have presented is used in certain combinations of orbital parameters and therefore not complete. Future research could be done

on scanning the all the phase-space coordinates. For instance we have taken the eccentricity to be zero in all cases of the IMBH configurations. This is not likely in the case of inspiraling cluster scenario unless the system is relaxed. In the case that the hidden IMBH is in circular orbit the Galactic plane offers the opportunity to hide an IMBH of up to $\sim 10^4$ $M_\odot$

The inspiraling cluster scenario itself is a limited solution to the "Paradox of Youth". It is show that it cannot account for all the S-stars at the GC. The inspiraling must proceed within 3 Myr otherwise the S-stars would loose their young appearance due to stellar evolution. Nevertheless, our study shows that due to the observational uncertainties in the orbital parameters of the S-stars, there is a window of opportunity for the inspiraling cluster scenario.

5.3 Where to go from here?

As long as the "Paradox of Youth" will lack a satisfactory solution and the uncertainties in the observational values are not better constrained, it will stay a point of discussion. The uncertainties in most of the observational data is due to the limit in accuracy of R_0. Future generations of large telescopes will restrain this uncertainty within a 0.1% value (Weinberg, Milosavljević & Ghez [74] and Weinberg, Milosavljević & Ghez. [75]). These telescopes will provide us with the values for the orbital parameters of up to a hundred S-stars. For our method this would lead to a much more sensitive system. On the other hand, the high accuracy will also constrain the dark mass to such a level that would render our method obsolete for this system.

Extending our method with the including of the other orbital parameters would be desirable. As the method would be completed it could be developed into a code that provides a probability density of dark objects in any system. Since there is yet no absolute evidence for the existence of IMBHs, our method could be used to scan for systems which could harbor these IMBHs.

Appendix A

Astronomical Values and Abbreviations

Unless stated otherwise:

G	Gravitational constant	$6.6742 \cdot 10^{-11}\, m^3 kg^{-1} s^{-2}$
c	speed of light	$2.99792458 \cdot 10^8\, ms^{-1}$
AU	Astronomical Unit	$149.5978875 \cdot 10^9\, m$
pc	parsec	$3.08568025 \cdot 10^{16} m$
$M_\odot$	Solar Mass	1.98892×10^{30} kg
ly	light year	9.4605284×10^{15} m

GC	Galactic Center
CM	Central Mass
R_0	Distance to Galactic Center
BH	Black Hole
IMBH	Intermediate Mass Black Hole
SMBH	Super Massive Black Hole
HVS	Hyper Velocity Stars
AGB	Asymptotic Giant Branch
IMF	Initial Mass Function
CND	Circum Nuclear Disk
VLA	Very Large Array
2MASS	2 Micron All Sky Survey
NICMOS	Near Infrared Camera and Multi-Object Spectrometer
HST	Hubble Space Telescope
IRAC	InfraRed Array Camera
ESO	European Southern Observatory
LBV	Luminous Blue Variable

Appendix B

Software

B.1 Kepler Code

The *Kepler* code can be obtained by sending an e-mail to: fgvandeuveren@planet.nl
The code is adjustable to the user's preferences. In order to make compiling easy a make file is added.
The code is implemented in a C++program called *orbit.cc*. It produces the positions and velocities of the S-stars by using the expressions derived in Chapter 2.

When initialising the code it can take input from the command-line:
-i input-filename (Input parameters)
-o output-filename
-dt accuracy
-g gif formatted snapshots

Note there is an animated gif available of the solutions of Chapter 2.

B.2 HNBody

The easiest way to get acquainted with the HNBody code is to take a look at the descriptive sample file 'sample.hnb'
How to run the code:

```
\$ hnbody inputfile.hnb
```

B.2.1 HNBody Input File

```
#####################################################################
#
# Sample HNBody Integration Input File.
#
```

```
# This file sets up a simple 3-body integration. Most of the file consists
# of explanatory comments describing the most important options. Options that
# have been commented out have the default values listed and can be omitted if
# the default is satisfactory; they are included here to orient the user as
# to what is available. The file does not include every possible option; the
# complete list of options is described in the options document.
#
#
#
# INTEGRATION PROPERTIES
#
#Integrator: Symplectic
#  choices are: Symplectic [Default], Burlisch-Stoer, Runge-Kutta
#  for B-S and R-K there is an optional second value, the accuracy to use
#                                                    (default: 1e-12)
#
# The following three options are meaningful only with Symplectic integrations;
# they specify the canonical coordinates and splitting to use, whether to
# utilize a symplectic corrector, and whether to follow close encounters:
#
#IntegCoord: Jacobi Order2 Kick-Drift
#  primary   values are: Jacobi (or Barycentric) [Default],
#  RegJacobi (or RegBarycentric), Bodycentric
#  secondary values are: Order2 [Default], Order4
#  tertiary  values are: Kick-Drift [Default], Drift-Kick, Shift-Drift
#
#Corrector: False
#  choices are: false/no [Default], true/yes, Order2, Order4, Order6
#               (true or yes means to use the highest available order)
#


# PROPERTIES OF INITIAL CONDITIONS

# The following options are all required; units can contain numbers
# and metric prefixes:
AngleUnit:  deg # base unit choices: deg, rad
LengthUnit: 5.2*AU # base unit choices: m, AU (or ua), pc
MassUnit:   2e27 kg # base unit choices: g, Msun
TimeUnit:   yr  # base unit choices: s, h, d, yr
StepSize:   0.01  # integration time step       (units of TimeUnit)
M  =  1 # mass of the dominant object (units of MassUnit)
N  =  3  # number of objects (including the dominant mass)

#OblateJ2 = 0 # J2 parameter of dominant mass (default is 0).
#OblateRadius = 0 # J2 radius    of dominant mass (default is 0).
#PostNewtonian: No # Include leading-order post-Newtonian corrections?
#   (default is false/no)


# INITIAL CONDITIONS

#   Specifying the initial conditions for each particle requires seven
#   numbers, its mass and six independent phase space coordinates. The
#   ordering and meaning of the seven required values is specified by
#   the InputOrder option, below. Units must be consistent with the units
#   declared above. If the Encounters option is enabled (see above), an
#   encounter radius (tag: EncRadius) must also be included in the initial
#   conditions. There are two basic input coordinate choices:
#
#   Elements are body-centered on the dominant mass; the dominant mass must
#   NOT be specified since elements are relative to its local rest frame.
```

```
#   The osculating orbital elements can be defined in numerous equivalent
#   representations; any six can be specified in InputOrder, so long as
#   they are independent.
#
#   Cartesian coordinates require that particle positions and velocities be
#   specified in some inertial reference frame. If the dominant mass is
#   not specified, it is assumed to be at rest at the origin; if it is
#   specified, its mass must match that given by the M option, above.
#
InputOrder: Mass SemiMajorAxis  Eccentricity Inclination \
 LongAscendNode ArgPeriapse  MeanAnomaly
#
# Tags ignore case and can be abbreviated (if unique);
# for example, you could write the above as:
#
#INPUTORD= mass semi ecc incl longasc argperi meananom
#
# alternate choices for elements:
#     PeriDistance, LongPeriapse, TrueLongitude, MeanLongitude,
#     TrueLatitude, MeanLatitude, TrueAnomaly, (Epoch, TimePeriapse)**
# Peri means periapse, Long means longitude, and Arg means argument.
# ** ( , ) means both are required if either is specified.
#
# The following would be a typical Cartesian example:
#
#InputOrder: x1 x2 x3 v1 v2 v3 mass
#
# InputOrder must also include EncRadius when Encounters are enabled.
#

# Here we specify the initial conditions:
#
#ParticleType: Default
#  choices are: HWPs [=Default], LWPs, ZWPs
#  (sets implied particle type for subsequent particle specifications)

0.001   5.2     0.0     0.0     0.0     0.0     0.0
0.001   6.0     0.0     0.0     0.0     0.0     0.0
#
# The above could also be written as: HWP = 0.001 5.2 ... etc.
#
# To include initial conditions (or anything else) from a file or files, use:
#
#Include: thisfile.hnb thatfile.hnb ...
#
# Output options are not required for initialization; the include mechanism
# makes it easy to maintain them separately:
#
include: output.hnb

#
# $Id: sample.hnb,v 1.2 2003/08/04 15:53:00 rauch Exp $
#
```

B.2.2 HNBody Output File

```
#
# $Id: output.hnb,v 1.3 2002/05/08 20:27:32 rauch Exp $
#
# HNBody output options (not required for initialization).
```

```
#
# All of the following items are optional. The four types of files are
# completely independent, but all require that Tfinal be defined. The Header,
# Digits, and Types items are optional (defaulting to True, 6, and all
# particles, respectively); all others are required if the associated file
# type is defined. Files not defined will not be written. Tfinal and all
# Intervals are in units of TimeUnit by default, or in units of StepSize if
# Steps is specified; in either case, values are rounded to the nearest
# integer multiple of the StepSize.
#

Tfinal  =  1000   # final integration time ([TimeUnit] or Steps)

#
# In OutputFiles, consecutive lines correspond to epochs separated by
# OutputInterval. A %d in the file name is replaced by the body's id number
# (if missing, the number is appended to the end). Bodies are numbered from 1
# in the order they were input, except that the dominant mass is always #0;
# this default can be overridden by specifying an IdTag in the InputOrder.
#
OutputFiles: body%d.dat # name of body-specific output files
OutputOrder: time x1 v3 ecc # data columns
OutputInterval: 10 # time interval for output ([TimeUnit] or Steps)
OutputCoord: Barycentric # output coordinate system
OutputHeader: True # Include column id codes and comments?
OutputDigits: 8 # precision of numbers in output
OutputTypes: HWPs # particle types to produce files for

#
# In StateFiles, each line corresponds to a single body; bodies are listed
# in order of their id tags (input order by default). A %d in the file name is
# replaced by the sequence number (with 0 corresponding to T = Tinitial);
# if missing, the number is appended to the end.
#
StateFiles: state%02d.dat # file to write system snapshots
StateOrder: x1 x2 x3 v1 v2 v3 # data columns
StateInterval: 2500 # interval to write state ([TimeUnit] or Steps)
StateCoord: Bodycentric # coordinate system
StateHeader: no # Include column id codes and comments?
StateDigits: 16 # precision of numbers
StateTypes: HWPs ZWPs  # particle types to include

#
# A SaveFile saves mutable integration data (in an unspecified format)
# to allow restoration upon crashes, power failures, etc. Note that restarting
# an integration also requires the original input file. A %d in the file name
# is replaced by the sequence number (with 0 corresponding to T = Tinitial);
# if omitted, the save file will be overwrittem each time.
#
SaveFiles: save%d.dat # Low-level save file to allow restarting
SaveInterval: 5000 # interval to save state ([TimeUnit] or Steps)

#
# EnergyFile has a fixed column format:
# Time  (E-E0)/E0  (Lx-Lx0)/L0 (Ly-Ly0)/L0 (Lz-Lz0)/L0
# E = total energy, Li = total angular momentum component
#
EnergyFile: energy.dat # file tracing system energy/angular momentum
EnergyHeader: True # Include column id comments?
EnergyInterval: 100 Steps # interval to write data ([TimeUnit] or Steps)
```

References

[1] S. Aarseth. Post-Newtonian N-body simulations. *Mon. Not. R. Astron. Soc.* ***378****, 285-292 (2007)*

[2] S. Aarseth. Black Hole Binary dynamics. astro-ph/0210116 v1 4 Oct 2002

[3] S. J. Aarseth, M. Hénon & R. Wielen. A Comparison of Numerical Methods for the Study of Star Cluster Dynamics. *Astronomy & Astrophysics* ***37****, 183-187 (1974)*

[4] R. D. Alexander, M. C. Begelman & P. J. Armitage. Constraints on the Stellar Mass Function from Stellar Dynamics at the Galactic Center. astro-ph/0609812 v1 29 Sep 2006

[5] A. M. Beloborodov, Y. Levin, F. Eisenhauer, R. Genzel, T. Paumerd, S. Gillessen & T. Ott. Clockwise Stellar Disk and the Dark Mass in the Galactic Center. astro-ph/0601273 v2 7 Jul 2006

[6] G. Battaglia, A. Helmi, H. Morrison, P. Harding, E. W. Olszewski, M. Mateo, K. C. Freeman, J. Norris & S. A. Shectman. The radial velocity dispersion profile of the Galactic halo: Constraining the density profile of the dark halo of the Milky Way. astro-ph/0506102 v2 10 Jul 2005

[7] J. Binney and S. Tremaine, *Galactic Dynamics*, Princeton University Press, 1987 N.J. isbn 0-691-08444-0

[8] P. J. Channell & C. Scovel. Symplectic integration of Hamiltonian systems. *Nonlinearity* ***3*** *231-259 (1990)*

[9] M. H. Christopher, N. Z. Scoville, S. R. Stolovy & Min S. Yun. HCN and HCO^+ Observations of the Galactic Circumnuclear Disk. *The Astrophysical Journal, Volume 622, Issue 1, pp. 346-365 March 2005*

[10] Y. Clénet, D. Rouan, D. Gratadour, F. Lacombe, E. Gendron, R. Genzel, T. Ott, R. Schödel & P. Léna. Detection of the Sgr A^* Activity at 3.8 and 4.8 μm with $NACO^*$. astro-ph/0407527 v1, 26 Jul 2004

[11] R. F. Coker & F. Melia, Hydrodynamical Accrection Onto Sgr. A^* From Distributed Point Sources. astro-ph/9708089 v1 10 Aug 1997

[12] G. W. Collins, II. The Virial Theorem in Stellar Astrophysics. *Astronomy and Astrophysics Series. Volume 7, 1978. 143 p.*

[13] J. Cuadra, S. Nayakshin, V. Springel & T. Di Matteo. Galactic Centre stellar winds and Sgr. A* Accretion. astro-ph/0505382 v2 9 Nov 2005

[14] M.B. Davies & A. King. The Stars at the Galactic Center. *The Astro Physical Journal, 624: L25 - L27, 2005 May 1*

[15] L. M. Dray, A. R. King & M. B. Davies. Young stars in the Galactic Centre: a potential intermediate-mass star origin. *Mon. Not. R. Astron. Soc. (2006), The Authors. Journal compilation, RAS*

[16] M. J. Duncan, H.F. Levison & M. H. Lee, A Multiple Time Step Symplectic Algorithm for Integrating Close Encounters. *The Astronomical Journal, 116:2067-2077, 1998 October*

[17] D. J. D. Earn. Symplectic integration without roundoff error. astro-ph/9408024 8 Aug 1994

[18] A. Eckart, R. Genzel, T. Ott & R. Schödel. Stellar Orbits near Sagittarius A*. astro-ph/0201031 v1 3 Jan 2002

[19] A. Eckart, T. Ott & R. Genzel. The Sgr A* Stellar Cluster: New NIR Imaging and Spectroscopy. astro-ph/9911011 v1, 2 Nov 1999

[20] F. Eisenhauer, R. Genzel, T. Alexander, R. Abuter, T. Paumard, T. Ott, A. Gilbert, S. Gillessen, M. Horrobin, S. Trippe, H. Bonnet, C. Dumas, N. Hubin, A. Kaufer, M. Kissler-Patig, G. Monnet, S. Ströbele, T. Szeifert, A. Eckart, R. Schödel & S. Zucker. SINFONI in the Galactic Center: young stars and IR flares in the central light month. astro-ph/0502129 Apr 2005

[21] F. Eisenhauer, R. Schödel, R. Genzel, T. Ott, M. Tecza, R. Abuter, A. Eckart & T. Alexander. A Geometric Determination of the Distance to the Galactic Center. *The Astrophysical Journal, 597:L121-L124, 2003 November 10*

[22] D. F. Figer, M. Morris, S. S. Kim & E. Serabyn. HST/NICMOS Imaging of the Quintuplet and Arches Clusters. *The Central Parsecs of the Galaxy, ASP Conference Series, Vol. 186. Edited by H. Falcke, A. Cotera, W. J. Duschl, F. Melia & M. J. Rieke. ISBN: 1-58381-012-9, 1999, p. 329*

[23] E. Forest & R. D. Ruth. Fourth-order symplectic integration. *Physica D 43: 105, 1990*

[24] R. Genzel, The Nuclear Star Cluster of the Milky Way: Star Formation, Dynamics and the Central Black Hole. astro-ph/0008119 v1 8 Aug 2000

[25] R. Genzel, R. Schödel, T. Ott, F. Eisenhauer, R. Hofmann, M. Lehnert, A. Eckart, T. Alexander, A. Sternberg, R. Lenzen, Y. Clénet, F. Lacombe, D. Rouan, A. Renzini & L. E. Tacconi-Garman. The Stellar Cusp around the Supermassive Black Hole in the Galactic Center. *The Astrophysical Journal, 594: 812-832, 2003 September 10*

[26] R. Genzel, C. Pichon, A. Eckart, O. E. Gerhard & T. Ott. Stellar Dynamics in the Galactic Centre: Proper motions and Anisotropy. astro-ph/0001428 v1, 25 Jan 2000

[27] A. M. Ghez, S. Salim, S. D. Hornstein, A. Tanner, J. R. Lu, M. Morris, E. E. Becklin & G. Duchêne. Stellar Orbits around the Galactic Center Black Hole. *The Astrophysical Journal, 620:744-757, 2005 February 20* astro-ph/0306130 v2 2 Nov 2004

[28] A. M. Ghez, S. D. Hornstein, J. Lu, A. Bouchez, D. Le Mignant, M. A. van Dam, P. Wizinowich, K. Matthews, M. Morris, E. E. Becklin, R.D. Campbell, J. C. Y. Chin, S. K. Hartman, E. M. Johansson, R. E. Lafon, P. J. Stomski & D. M. Summers. The First Laser Guide Star Adaptive Optics Observations of the Galactic Center: Sgr. A*'s Infrared Color and the Extended Red Emission in its Vicinity. *ApJ, Vol. 635, 20 Dec 2005*

[29] A. M. Ghez, B. L. Klein, M. Morris & E. E. Becklin. High Proper Motion Stars in the Vicinity of Sgr. A*: Evidence for a Supermassive Black Hole at the Center of our Galaxy. astro-ph/9807210 v2, 21 Juli 1998

[30] A. M. Ghez, E. Becklin, G. Dûchene, S. Hornstein, M. Morris, S. Salim & A. Tanner. Full Three Dimensional Orbits for Multiple Stars on Close Approaches to the Center SMBH. astro-ph/0303151 v1, 7 March 2003

[31] A. M. Ghez, G. Duchêne, K. Matthews, S. D. Hornstein, A. Tanner, J. Larkin, M. Morris, E. E. Becklin, S. Salim, T. Kremenek, D. Thompson. B. T. Soifer, G. Neuge-Bauer & I. McLean. The First Measurement of Spectral Lines in a Short-Period Star Bound to the Galaxy's Central Black Hole: A Paradox of Youth. *The Astrophysical Journal, 586:L127-L131, 2003 April 1*

[32] I. Ginsburg & A. Loeb. Hypervelocity Collisions of Binary Stars at the Galactic Centre. astro-ph/0609440 v2 11 Jan 2007

[33] M. Atakan Gürkan & F. A. Rasio. The Disruption of Stellar Clusters Containing Massive Black Holes near the Galactic Center. arXiv:astro-ph/0412452 4 Apr 2005

[34] B. M. S. Hansen & M. Milosavljević. The Need for a Second Black Hole at The Galactic Center. *The Astrophysical Journal, 593:L77L80, 2003 August 20*

[35] D.C. Heggie and R.D. Mathieu, Standardised Units and Time Scales. p233 of *The Use of Supercomputers in Stellar Dynamics*, edited by S. McMillan and P. Hut, 1986 Springer

[36] T. Ito & K. Tanikawa. Long-term integrations and stability of planetary orbits in our Solar system. *Mon. Not. R. Astron. Soc.* ***336****, 483-500 (2002)*

[37] M. Iwasawa, Y. Funato & J. Makino. Evolution of Massive Blackhole Triples I – Equal-mass binary-single systems. astro-ph/0511391 v1 14 Nov 2005

[38] J. A. Kollmeier & A. Gould, Where are the Old-Population High Velocity Stars? astro-ph/0701350 v1 11 Jan 2007

[39] A. Krabbe, R. Genzel, A. Eckart, F. Najarro, D. Lutz, M. Cameron, H. Kroker, L. E. Tacconi-Garman, N. Thatte, L. Weitzel, S. Drapatz, T. Geballe, A. Sternberg & R. Kudritzki. The Nuclear Cluster of the Milky Way: Star Formation and Velocity Dispersion in the Central 0.5 Parsec. *The Astrophysical Journal, 447 : L 95 - L 99, 1995 July 10*

[40] E. Kreyszig, *Advanced Engineering Mathematics 8th edition*, J. Wiley & Sons, Inc. isbn 0-471-33328-x 1999 page 382 section 7.3

[41] C. C. Lang, M. Morris & L. Echevarria. A Radio Polarimetric Study of the Galactic Center Threads. *The Astrophysical Journal, 526:727-743, 1999 December 1*

[42] Y. Levin & A. M. Beloborodov. Stellar disk in the galactic center – a remnant of a dense accretion disk? astro-ph/0303436

[43] J. R. Lu, A. M. Ghez, S. D. Hornstein, M. Morris & E. E. Becklin. IRS-16SW a New Comoving Group of Young Stars in the Central Parsec of the Milky Way. astro-ph/0504276 v1 12 April 2005

[44] J. P. Maillard, T. Paumard, S. R. Stolovy & F. Rigaut. The nature of the Galactic Center source IRS 13 revealed by high spatial resolution in the infrared. *Astronomy & Astrophysics 423 (2004) 155-167* astro-ph/0404450 v1 22 Apr 2004

[45] J. Makino, P. Hut, M. Kaplan & H. Saygin. A Time-Symmetric Block Time-Step Algorithm for N-Body Simulations, New Astron 12, 124 2006. astro-ph/0604371 v2 26 May 2006

[46] F. Martins, R. genzel, D. J. Hillier, F. Eisenhauer, T. Paumard, S. Gillessen, T. Ott & S. Trippe. Stellar and Wind properties of massive stars in the central parsec of the Galaxy. *Astronomy & Astrophysics manuscript no. martins ESO 2007* astro-ph/0703211 v1 9 March 2007

[47] M. Micic, K. Holley-Bockelmann, S. Sigurdsson & T. Abel. Supermassive Black Hole Growth and Merger Rates from Cosmological N-body Simulations. astro-ph/0703540 v1 20 Mar 2007

[48] J. Miralda-Escudé & A. Gould. A Cluster of Black Holes at the Galactic Center. *The Astrophysical Journal, 545:847-853, 2000 December 20*

[49] T. Morris & P. Podsiadlowski. The Triple-Ring Nebula around SN1987A. astro-ph 0703317, 13 Mar/May 2007

[50] M. Morris & S. Nayakshin. News from the 2006 GC Workshop. astro-ph/0701047 v1, 2 Jan 2007

[51] M. Morris. The Galactic Center Magnetosphere. astro-ph/0701050 v1 2 Jan 2007

[52] S. Nayakshin, J. Cuadra & V. Springel. Simulations of Star Formation in a Gaseous Disc Around Sgr. A* - a failed Active Galactic Nulceus. astro-ph/0701411 v1 5 Jan 2007

[53] S. Nayakshin, W. Dehnen, J. Cuadra & R. Genzel. Weighing the Young Stellar Discs around Sgr. A*. astro-ph/0502129.astro-ph/0511830 v1 30 Nov 2005

[54] R. M. O'Leary & A. Loeb. Production of Hypervelocity Stars through Encounters woth Stellar-Mass Black Holes in the Galactic Centre. astr-ph/0609046 v1 1 Sep 2006.

[55] L. Pasquini , P. Bonifacio , S. Randich , D. Galli & R. G. Gratton. Beryllium in turnoff stars of NGC6397: early Galaxy spallation, cosmochronology and cluster formation*. astro-ph/0407524 v1 26 Jul 2004

[56] T. Paumard, R. Genzel, F. Martins, S. Nayakshin, A. M. Beloborodov, Y. Levin, S. Trippe, F. Eisenhauer, T. Ott, S. Gillessen, R. Abuter, J. Cuadra, T. Alexander & A. Sternberg. The Two Young Star Disks in Central Parsec of the Galaxy: Properties, Dynamics and Formation. astro-ph/0601268 v2 3 Feb 2006

[57] S. F. Portegies Zwart, S. L. W. McMillan & O. Gerhard. The origin of IRS 16: dynamically driven inspiral of a dense star cluster to the Galactic center? astro-ph/0303599 v2 1 Apr 2003

[58] J. Pott, A. Eckart, A. Glindemann & R. Schödel. First infrared VLTI fringes on Galactic Center sources. Journal of Physics: Conference Series **54** (2006) 273-278. Gaxy Center Workshop.

[59] T. Quinn, N. Katz, J. Stadel & G. Lake. Time stepping N-body simulations. astro-ph/9710043 v1 3 Oct 1997

[60] S. Ramstedt, F. L. Schöier, H. Olofsson & A. A. Lundgren. Massloss Properties of S-Stars on the AGB. astro-ph/0605664 v1, 26 May 2006

[61] K. P. Rauch & D. P. Hamilton. The HNBody Package for Symplectic Integration of Nearly-Keplerian Systems. *American Astronomical Society, DDA Meeting #33, #08.02; Bulletin of the American Astronomical Society, Vol. 34, p.938*

[62] M.J. Reid, K. M. Menten, R. Genzel, T. Ott, R. Schödel & A. Brunthaler. The Position, Motion and Mass of Sgr. A*. astro-ph/0304095 4 Apr 2003

[63] M. J. Reid. The distance to the center of the Galaxy. *Annual review of astronomy and astrophysics. Vol. 31 (A94-12726 02-90), p. 345-372. 1993*

[64] M. J. Reid & A. Brunthaler. The Proper Motion of Sgr A*: II. The Mass of Sgr A*. astro-ph/0408107 v1 5 Aug 2004

[65] G. F. Rubilar & A. Eckart. Periastron shifts of stellar orbits near the Galactic Center. *Astronomy & Astrophysics **374**, 95-104 (2001)*

[66] P. Saha & S. Tremaine. Symplectic Integrators for Solar System Dynamics. *The Astronomical Journal, volume 104, number 4, 1992*

[67] R. Schödel, A. Eckart, T. Alexander, D. Merritt, R. Genzel, A. Sternberg, L. Meyer, F. Kull, J. Moultaka, T. Ott & C. Straubmeier. The Structure of the Nuclear Stellar Cluster of the Milky Way. *Astronomy & Astrophysics **469**, 125-146 (2007)*

[68] R. Schödel, R. Genzel, T. Ott & A. Eckart. The Galactic Center Stellar Cluster: The Central Arcsecond. astro-ph/0304197 v1 10 Apr 2003

[69] R. Schödel, A. Eckart, C. Iserlohe, R. Genzel & T. Ott. A Black Hole in the Galactic Center Complex IRS 13E?. astro-ph/0504474 v1 21 Apr 2005

[70] S. R. Stolovy, T. L. Hayward & T. Herter. The First Mid-Infrared Detection of a Source Coincident with Sagittarius A*. *Astrophysical Journal Letters, volume 470, p. L 45*

[71] Z. Shen, K. Y. Lo, M.-C. Liang, P. T. P. Ho & J.-H. Zhao. A size of 1 AU for the radio source Sgr. A* at the centre of the Milky Way. astro-ph 0512515 v2, 26 Dec 2005

[72] L. Šubr & V. Karas, On highly eccentric stellar trajectories interacting with a self-gravitating disc in Sgr.A*, *Astronomy & Astrophysics manuscript no. s02corr, March 15, 2007*

[73] A. Tanner, D. F. Figer, F. Najarro, R. P. Kudritzki, D. Gilmore, M. Morris, E. E. Becklin, I. S. McLean, A. M. Gilbert, J. R. Graham, J. E. Larkin, N. A. Levenson & H. I. Teplitz. High Spectral Resolution Observations of the Massive Stars in the Galactic Center. *The Astrophysical Journal, volume 641, part 1 (2006), pages 891904*

[74] N. Weinberg, M. Milosavlević & A. Gehz. Astrometric Monittoring of Stellar Orbits at the Galactic Center with a Next Generation Large Telescope Astrometry in the Age of the Next Generation of Large Telescopes. *ASP Conference Series, Vol. 338, 2005* astro-ph/0512621 v2 30 Dec 2005

[75] N. Weinberg, M. Milosavljević & A. M. Ghez. Stellar Dynamics at the Galactic Center with an Extremely Large Telescope. astro-ph/0404407 v2, 29 Dec 2005

[76] H. Yoshida. Construction of higher order symplectic integrators. *Phys. Lett. A 150, 262, 1990*

[77] K. Zhang & D. P. Hamilton. Orbital resonances in the inner neptunian system I. The 2:1 Proteus-Larissa mean-motion resonance. *ScienceDirect, Icarus 188 (2007) 386-399*